JEM Journal of Experimental Medicine

ARTICLE

Wnt5a induces and maintains prostate cancer cells dormancy in bone

Dong Ren[1,2,3*], Yuhu Dai[1,3*], Qing Yang[1,3*], Xin Zhang[2,4], Wei Guo[1,3], Liping Ye[2], Shuai Huang[1,3], Xu Chen[5], Yingrong Lai[6], Hong Du[7], Chuyong Lin[2], Xinsheng Peng[1,3], and Libing Song[2,8]

In a substantial fraction of prostate cancer (PCa) patients, bone metastasis appears after years or even decades of latency. Canonical Wnt/β-catenin signaling has been proposed to be implicated in dormancy of cancer cells. However, how these tumor cells are kept dormant and recur under control of Wnt/β-catenin signaling derived from bone microenvironment remains unknown. Here, we report that Wnt5a from osteoblastic niche induces dormancy of PCa cells in a reversible manner in vitro and in vivo via inducing Siah E3 Ubiquitin Protein Ligase 2 (SIAH2) expression, which represses Wnt/β-catenin signaling. Furthermore, this effect of Wnt5a-induced dormancy of PCa cells depends on receptor tyrosine kinase-like orphan receptor 2 (ROR2), and a negative correlation of ROR2 expression with bone metastasis–free survival is observed in PCa patients. Therefore, these results demonstrate that Wnt5a/ROR2/SIAH2 signaling axis plays a crucial role in inducing and maintaining PCa cells dormancy in bone, suggesting a potential therapeutic utility of Wnt5a via inducing dormancy of PCa cells in bone.

Introduction

Prostate cancer (PCa) is one of the most common malignancies in men worldwide (Siegel et al., 2018) and is characterized by its high incidence of bone metastasis (Roodman, 2004). Intriguingly, metastatic bone tumors can appear years and even decades later, following excision of primary PCa (Pound et al., 1999). Experimental studies have shown that the efficiency of metastatic tumor formation after intravenous injection of tumor cells was as low as 0.01% (Fidler, 1970), which may be explained by entrance of cancer cells into a dormant state (Luzzi et al., 1998). Lambert et al. (2017) propose a viewpoint that when tumor cells arrive in a new unfamiliar microenvironment to which they are poorly adapted, they are likely to enter into a prolonged growth-arrested state. Therefore, an in-depth understanding of the mechanism underlying cancer dormancy will be helpful for prevention and treatment of metastatic tumor.

In different types of cancer, tumor cells preferentially metastasize to the selected organs, referred to as the "seed and soil" theory (Paget, 1989). Emerging evidence has reported that tumor cells are often found in a dormant state, which is, to some extent, determined by the interactions between the tumor cells and signals within specific niche microenvironments (Ebinger et al., 2016; Price et al., 2016). Induction of cancer dormancy is initiated by a variety of events in the microenvironmental niche, such as angiogenic balance (Naumov et al., 2006), immunological equilibrium (Koebel et al., 2007), and stress signaling (Lu et al., 2008). In bone metastasis of cancer, the fate of colonizing tumor cells is likely to be determined by their location in bone microenvironments: tumor cells arriving in the bone-remodeling compartment (<20% of endosteal bone surface), which is the zone of active bone remodeling, are exposed to a rich microenvironment containing pro-growth factors and thus grow immediately after colonization. However, those colonized in the inactive surfaces (~80% of the endosteal bone surface) implant in a quiescent microenvironment that promotes tumor cells dormancy (Andersen et al., 2009; Croucher et al., 2016). Therefore, it is conceivable that colonizing tumor cells are more likely to be dormant when they arrest in bone. Indeed, several lines of investigation showed that osteoblastic niche plays an important role in controlling dormancy of tumor cells (Lawson et al., 2015). Although the dormancy-promoting role of osteoblastic niche has

[1]Department of Orthopedic Surgery, the First Affiliated Hospital of Sun Yat-sen University, Guangzhou, China; [2]Department of Experimental Research, State Key Laboratory of Oncology in Southern China, Sun Yat-sen University Cancer Center, Guangzhou, China; [3]Guangdong Provincial Key Laboratory of Orthopedics and Traumatology, Guangzhou, China; [4]Clinical Experimental Center, Jiangmen Central Hospital, Affiliated Jiangmen Hospital of Sun Yat-sen University, Jiangmen, China; [5]Department of Urology, the First Affiliated Hospital of Sun Yat-sen University, Guangzhou, China; [6]Department of Pathology, the First Affiliated Hospital of Sun Yat-sen University, Guangzhou, China; [7]Department of Pathology, the First People's Hospital of Guangzhou City, Guangzhou, China; [8]Key Laboratory of Protein Modification and Degradation, School of Basic Medical Sciences, Affiliated Cancer Hospital and Institute of Guangzhou Medical University, Guangzhou, China.

*D. Ren, Y. Dai, and Q. Yang contributed equally to this paper; Correspondence to Libing Song: songlb@sysucc.org.cn; Xinsheng Peng: pengxs66@yahoo.com.

been elucidated, crucial signals supporting cancer dormancy remain to be further clarified.

Accumulating studies have indicated that inactivation or down-regulation of pro-proliferation signaling contributes to cancer cell dormancy (White et al., 2004; Lu et al., 2008; Dey-Guha et al., 2011). Furthermore, factors secreted by osteoblastic niche, including IL6, growth arrest specific protein 6 (GAS6), and bone morphogenetic proteins, play critical roles in cancer dormancy (Karadag et al., 2000; Ro et al., 2004; Døsen et al., 2006; D'Souza et al., 2012). Notably, a study from Nemeth showed that Wnt5a maintained hematopoietic stem cells (HSCs) in a quiescent G_0 state via inhibiting Wnt3a-mediated canonical Wnt signaling (Nemeth et al., 2007), and activity of canonical Wnt signaling has been recently demonstrated to generally be inversely associated with the dormancy of colorectal cancer cells (Buczacki et al., 2018). Importantly, Shiozawa et al. (2011) have demonstrated that disseminated PCa cells colonize and occupy the same osteoblastic niche via competing with HSCs. Therefore, we hypothesize that Wnt5a may play a similar role in the maintenance of disseminated PCa cells dormancy as it does in HSCs. In this study, our results demonstrate that Wnt5a from osteoblastic niche induces dormancy of PCa cells via activation of noncanonical ROR2/SIAH2 signaling, resulting in repression of canonical Wnt/β-catenin signaling, suggesting a potential therapeutic utility of Wnt5a in the dormancy of PCa cells in bone.

Results

Osteoblasts repress the growth of PCa cells

Osteoblasts, a primary component of osteoblastic niche, have been reported to maintain cells colonized in the osteoblastic niche in a quiescent state (Wang et al., 2014), and cells isolated from osteoblast-ablated mice show a loss of quiescence (Bowers et al., 2015). Therefore, we further investigated whether dormancy of PCa cells was induced via co-culture with osteoblasts. Primary osteoblasts from the calvaria of neonatal rats were first isolated (Fig. S1 A), and different staining methods were used in primary rat osteoblast cultures (Fig. S1, B–D). Then, we further co-cultured PCa cells and primary osteoblasts in a transwell plate (Fig. 1 A, top panel) and found that the cell numbers were significantly decreased (Fig. 1 B). Consistently, the number of PCa cells were reduced when cultured in the conditioned medium from osteoblast (Fig. 1 A, bottom panel; and Fig. S1 E). Furthermore, the number of Ki-67–positive populations and cyclinD1 and cyclinE1 expression were repressed when co-cultured with osteoblasts or cultured in the conditioned medium from primary osteoblast (PrOB-CM); conversely, the percentage of cells in the G_0/G_1 phase and p21 and p27 expression were enhanced (Fig. 1, C–F). These results indicate that osteoblasts suppress proliferation and retard cell cycle progression in PCa cells.

Wnt5a is essential for the low proliferation ability of PCa cells within the osteoblastic niche

Wnt signaling within the bone microenvironment plays a crucial role in the equilibrium of cell dormancy and reactivation (Trowbridge et al., 2010; Amin et al., 2016). To discern the relevant Wnt signaling derived from osteoblasts, we first examined the mRNA expression levels of Wnt proteins in primary osteoblast and found that mRNA expression of several noncanonical Wnt ligands, including *Wnt5a*, *5b*, *11*, and *16*, was dramatically elevated in osteoblast (Fig. 2 A), suggesting that osteoblast-induced tumor cell dormancy may be associated with noncanonical Wnt signaling. The ELISA results showed that the concentration of Wnt5a, 5b, 11, and 16 was at a much higher level in the supernatant of osteoblasts, but hardly detectable in that of PCa cells, except for Wnt11 (Fig. 2 B), suggesting that primary sources of Wnt ligands within osteoblastic niche are osteoblasts rather than the cancer cells themselves. To determine which factor is responsible for the inhibitory effect of osteoblasts on the proliferation of PCa cells, the effect of recombinant human proteins of these Wnt ligands on Ki-67$^+$ cells number was first investigated. As shown in Fig. 2 C and Fig. S2 (A and B), only Wnt5a (>100 ng/ml) differentially decreased the Ki-67$^+$ populations and cyclinD1 and cyclinE1 expression and increased p21 and p27 expression.

We further knocked down *Wnt5a* expression in osteoblast to investigate whether silencing *Wnt5a* restores the growth ability of PCa cells (Fig. S2, C and D). As shown in Fig. 2 (D–F), the proliferation ability and cell cycle of PCa cells co-cultured with PrOB-CM from *Wnt5a*-silenced osteoblasts were increased. Furthermore, our results revealed that Wnt5a was also detected in the supernatant of MC3T3-E1, hFOB1.19, and bone marrow–derived mesenchymal stem cells (BMSCs) and the number of Ki-67$^+$ PCa cells was reduced in the presence of PrOB-CM from each of these cell types (Fig. S2, E and F). Importantly, silencing *Wnt5a* in these cell types enhanced the number of Ki-67$^+$ cells repressed by the PrOB-CM from vector cells (Fig. 2 G and Fig. S2, G and H), indicating that the various sources of Wnt5a from multiple cell types within the osteoblastic niche inhibits the proliferation of PCa cells. Therefore, these data indicate that Wnt5a from osteoblastic niche induces metastatic dormancy.

Wnt5a elicits dormancy of PCa cells in a reversible manner

To investigate the effect of Wnt5a on the dormancy of PCa cells, we first stained PCa cells with vital lipophilic fluorescent dyes (DiD), as the intensity of DiD staining declines with dividing of cells (Wang et al., 2015; Sharma et al., 2016). Immunofluorescence staining revealed that Wnt5a maintained the number of DiD$^+$ cells (red) and reduced the number of Ki-67$^+$ cells (green: FITC) over time (Fig. 3, A–C). Dormant cancer cells were characterized by regaining proliferation ability after withdrawing the dormancy-inducing factor. Therefore, we further withdrew Wnt5a on day 4 and found that the number of Ki-67$^+$ cells increased on day 6; conversely, the number of DiD$^+$ cells decreased (Fig. 3, A–C). Furthermore, the inhibitory effects of Wnt5a on cell proliferation, Ki-67$^+$ cell population, and cell cycle were reversed after withdrawal of Wnt5a (Fig. 3, D–F). Therefore, our results indicate that Wnt5a induces dormancy of PCa cells in vitro in a reversible manner.

To discern mitotically quiescent cells in vivo, a mouse model of bone metastasis was used, where DiD-labeled and luciferase-expressing PC-3 cells were inoculated into the left cardiac ventricle of mice (Fig. 4 A). Wnt5a was injected daily through the lateral tail vein before 3 d of cell inoculation. Systemic administration of Wnts ligands has been reported to have subsequent

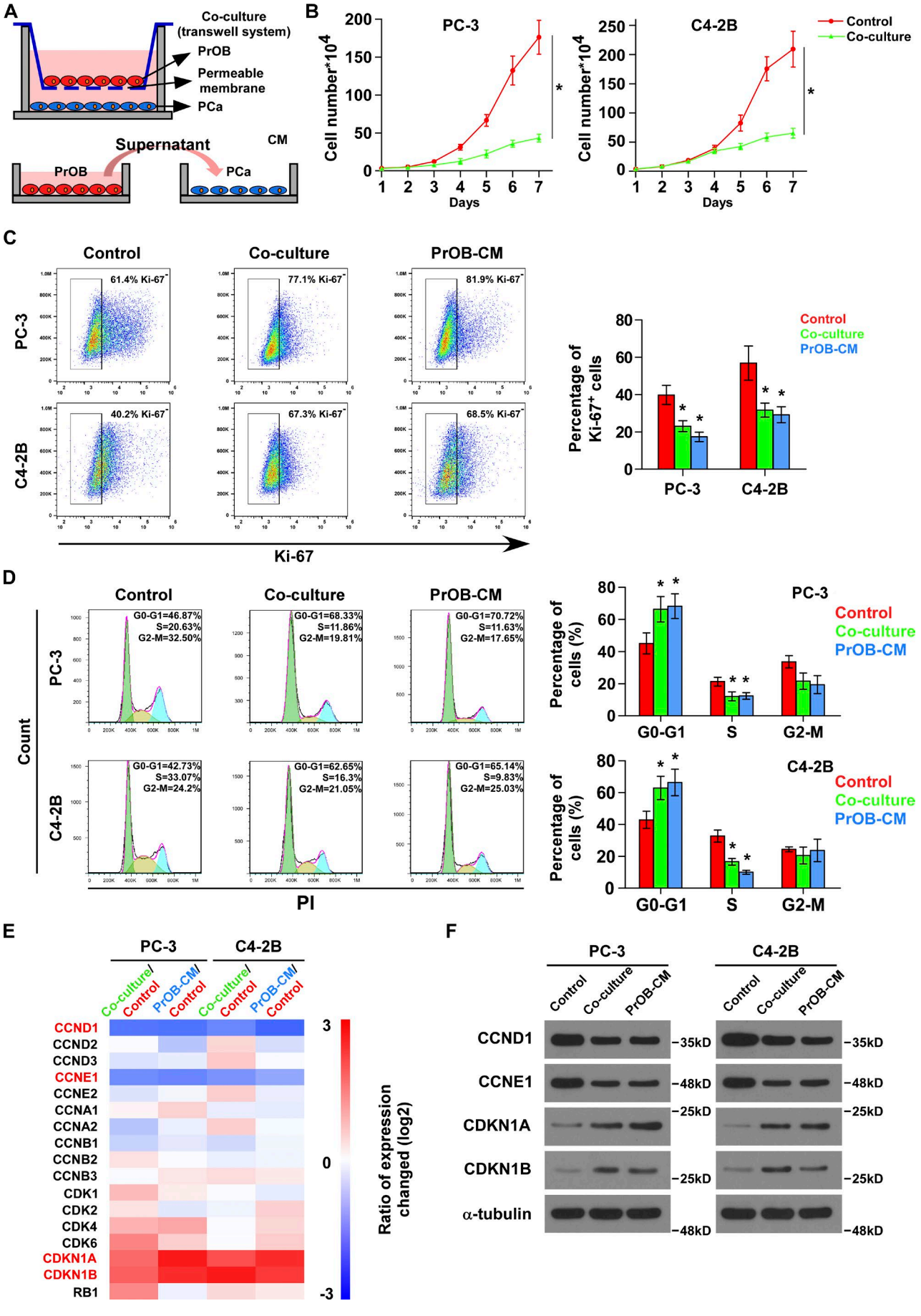

effects in vivo (Kim et al., 2009). Equivalent numbers of double DiD-labeled (DiD$^+$: red) and luciferase-expressing (luciferase$^+$: green) cells were observed in the tibiae of mice from different groups on day 2 (Fig. 4 B). Mice were culled after 10–12 wk of injection of PC-3 cells, and the tibiae were collected and processed for confocal microscopy. At this stage, the tibiae of mice with consecutive injection of Wnt5a exhibited a higher frequency of double DiD$^+$ and luciferase$^+$ cells and no obvious bone lesions compared with control group (Fig. 4, C–G). Importantly, withdrawal of Wnt5a on day 41 significantly decreased the number of double DiD$^+$/luciferase$^+$ tumor cells and increased the luciferase$^+$ tumor cells, which showed the obvious osteolytic bone tumors on day 80 (Fig. 4, C–G). Collectively, these results demonstrate that Wnt5a induces dormancy of PCa cells in bone in a reversible manner in vivo.

Wnt5a inhibits osteolytic bone destruction of PCa cells in vivo

To determine the effect of Wnt5a on bone metastasis of PCa in vivo, the luciferase-labeled PC-3 cells were inoculated into the left cardiac ventricle of mice to monitor development of bone metastatic tumors. As shown in Fig. 5 (A and B), PC-3 cells treated with Wnt5a displayed fewer bone metastatic sites than control group. H&E staining showed that Wnt5a dramatically reduced the tumor burden in bone (Fig. 5 C). Furthermore, the mice treated with Wnt5a displayed fewer bone metastatic foci, smaller osteolytic areas, and longer bone metastasis–free survival (Fig. 5, D–F). Importantly, the mice withdrawing Wnt5a on day 41 exhibited more bone metastatic foci, tumor burden, and shorter bone metastasis–free survival compared with those with continuous Wnt5a treatment group on day 80 (Fig. 5, A–F). These findings indicate that Wnt5a inhibits bone metastasis of PCa cells in a reversible manner in vivo.

To test the therapeutic efficacy of Wnt5a in vivo, Wnt5a was administered on day 41, when metastatic bone tumors were observed in most of the mice according to the bioluminescent imaging (BLI) signals (Fig. 5 A). As shown in Fig. 5 (A–F), administration of Wnt5a on day 41 had no significant effect on bone metastatic tumor compared with the control groups. In intratibial injection model, the left tibial bone of the mice was injected with PC-3 cells to form bone tumors around 21 d, according to the BLI signals (Fig. 5 G). Then, the left tibia was shielded to avoid the effect of the established BLI signal in the left tibia on the BLI signal of the right tibiae when the right tibiae were injected with the same number of PC-3 cells on day 25 (Fig. 5 G). Wnt5a was injected daily through the lateral tail vein before 3 d of cell injection into the right tibia (Fig. 5 G). Interestingly, we found that Wnt5a treatment resulted in significant reduction in tumor burden of right tibia compared with that in the left tibia on day 46 (Fig. 5, G–K). We posited that this may be due to the phenomenon of the "vicious cycle," namely the formation of metastatic bone tumors resulted in the release of several cytokines from the bone matrix during lysis, particularly TGF-β, promoting the proliferation and survival of tumor cells within bone microenvironment (Kingsley et al., 2007; Ell and Kang, 2012). To confirm this hypothesis, three different treatment regimens, including Wnt5a, TGF-β receptor 1 inhibitor SD208, and Wnt5a + SD208, were administered on day 41 after formation of osteolytic bone tumors. After 6 wk of treatment, Wnt5a with SD208 significantly reduced the osteolytic area compared with Wnt5a treatment alone (Fig. 5, L–P). However, Wnt5a + SD208 did not exhibit more efficacy than SD208 alone (Fig. 5, L–P). Thus, these findings indicate that Wnt5a inhibits bone metastasis of PCa cells in a preventive manner in vivo.

Dormant cells induced by Wnt5a exhibit resistance to docetaxel

Since dormant cells are known for their resistance against drug treatment, we further investigated the effect of chemotherapy on Wnt5a-induced dormant cells in bone using docetaxel, the most commonly used drug for the treatment of bone metastatic PCa (Banerjee et al., 2007; Yang et al., 2018). First, antimetastatic efficacy of docetaxel in bone metastasis of PCa was demonstrated by the finding that the tumor burden of mice treated with docetaxel was significantly reduced compared with that in the vehicle (Fig. 6, A–E). Next, the effect of docetaxel on dormant PCa cells was further investigated. As shown in Fig. 6 (F–I), the tibiae of the mice cotreated with docetaxel and Wn5a did not show the developed bone metastasis and displayed a similar number of double DiD$^+$/luciferase$^+$ tumor cells, compared with that in the mice treated with Wnt5a alone. Importantly, removal of both docetaxel and Wn5a on day 57 resulted in quick development of bone tumors on day 100, which was also observed in the mice removed of Wnt5a (Fig. 6, J–N). Collectively, these results further supported the notion that PCa cells entered into a dormant state in bone in the presence of Wnt5a and survived under treatment of docetaxel.

Wnt5a inhibits Wnt/β-catenin signaling independent of Wnt/Ca^{2+} pathways

Wnt5a represses canonical Wnt activity in different species (Torres et al., 1996; Kühl et al., 2000; Ishitani et al., 2003). Thus, we further investigated whether Wnt5a inhibited Wnt/β-catenin signaling in PCa cells. As shown in Fig. 7 (A–C), Wnt5a reduced the total expression and nuclear translocation of β-catenin, TOP/FLASH activity, and downstream target genes expression in the absence or presence of Wnt3a stimulation. Wnt5a has been identified to be involved in the stimulation of intracellular Ca^{2+}

Figure 1. **Primary osteoblasts repressed the growth of PCa cells. (A)** The model of PCa cell co-culture with primary osteoblast in the transwell plate (co-culture; top) or cultured in PrOB-CM (bottom). **(B)** PC-3 and C4-2B cells were co-cultured with osteoblasts in a co-culture transwell system followed by quantifying cell number. Mean ± SD; *, P < 0.05 by ANOVA for repeated measures. **(C)** PCa cells were used for flow cytometry analysis of Ki-67 marker on day 5 in the indicated groups. Histograms showed the proportion of Ki-67$^+$ cells in each groups. Mean ± SD; *, P < 0.05 by one-way ANOVA. **(D)** Flow cytometry analysis of cell cycle in the indicated groups on day 5. Mean ± SD; *, P < 0.05 by one-way ANOVA. **(E)** Real-time PCR analysis of multiple cell cycle regulators expression in the indicated groups on day 5. Pseudo-color scale values were log2 transformed. Transcript levels were normalized by GAPDH expression. The experiment was independently performed three times. **(F)** Western blotting analysis of cyclin D1, cyclin E1, CDKN1A (p21), and CDKN1B (p27) expression in the indicated groups on day 5. α-Tubulin served as the loading control. The experiment was independently performed three times.

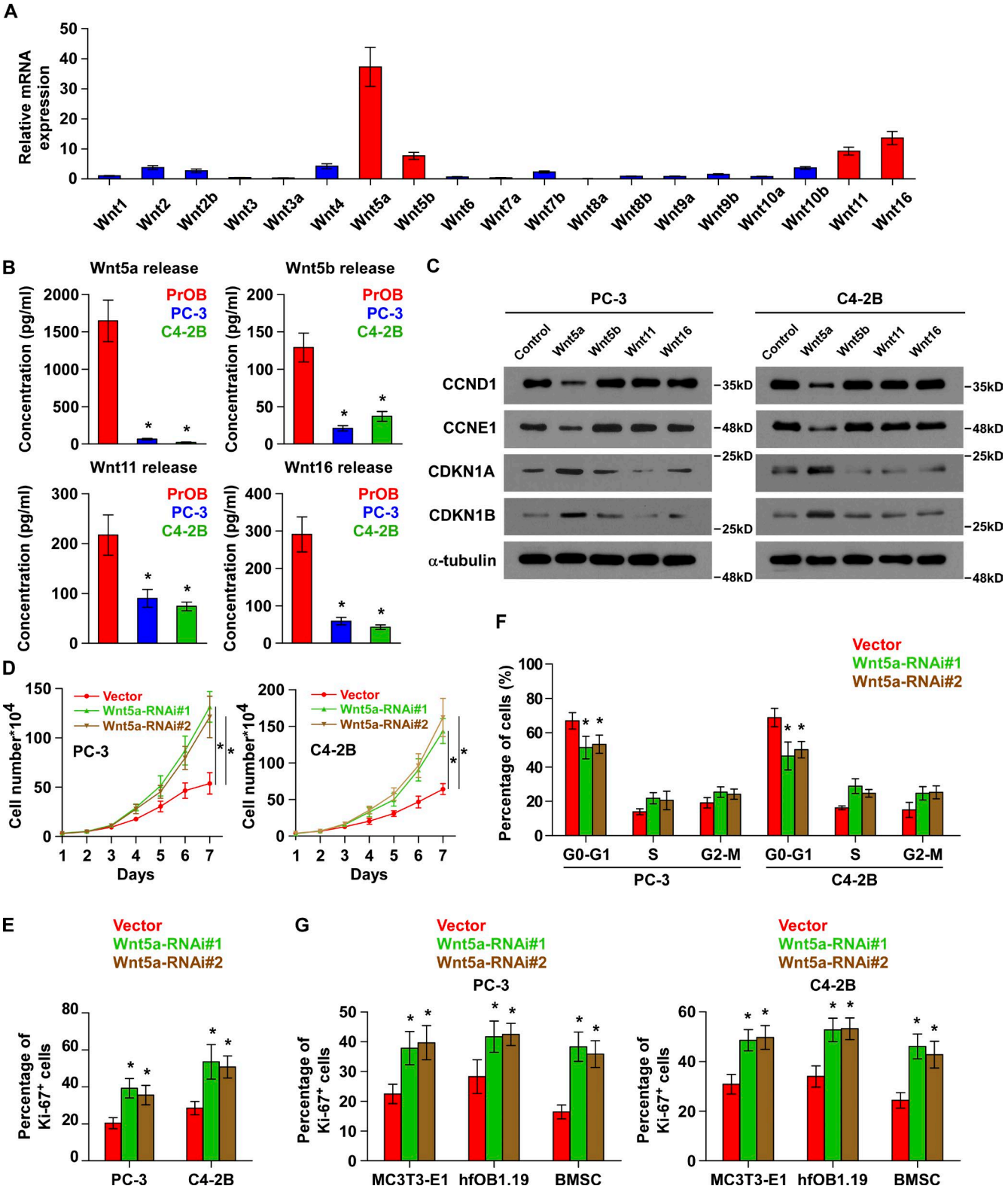

Figure 2. **Wnt5a inhibits proliferation and retards cell cycle progression of PCa cells. (A)** Real-time PCR analysis of Wnt mRNA expression in primary osteoblasts. Red bars show the mRNA expression of Wnt with both a fivefold-change increase and statistical significance ($P < 0.05$ by one-way ANOVA), compared with mRNA expression of Wnt1. Blue bars represent the mRNA expression of Wnt with no more than fivefold-change increase compared with mRNA expression of Wnt1. Mean ± SD. **(B)** The concentration of Wnt5a, 5b, 11, and 16 in the supernatant of the indicated cells by ELISA. Mean ± SD. *, $P < 0.05$ by one-way ANOVA. **(C)** Western blotting analysis of cyclin D1, cyclin E1, p21, and p27 expression in the indicated PCa cells. α-Tubulin served as the loading control. The experiment was independently performed three times. **(D–F)** The cell number, percentage of Ki-67$^+$ cells, and cell cycle analysis in the indicated PCa cells. Mean ± SD; *, $P < 0.05$ by one-way ANOVA. **(G)** The percentage of Ki-67$^+$ cells in the indicated PCa cells. Mean ± SD; *, $P < 0.05$ by one-way ANOVA.

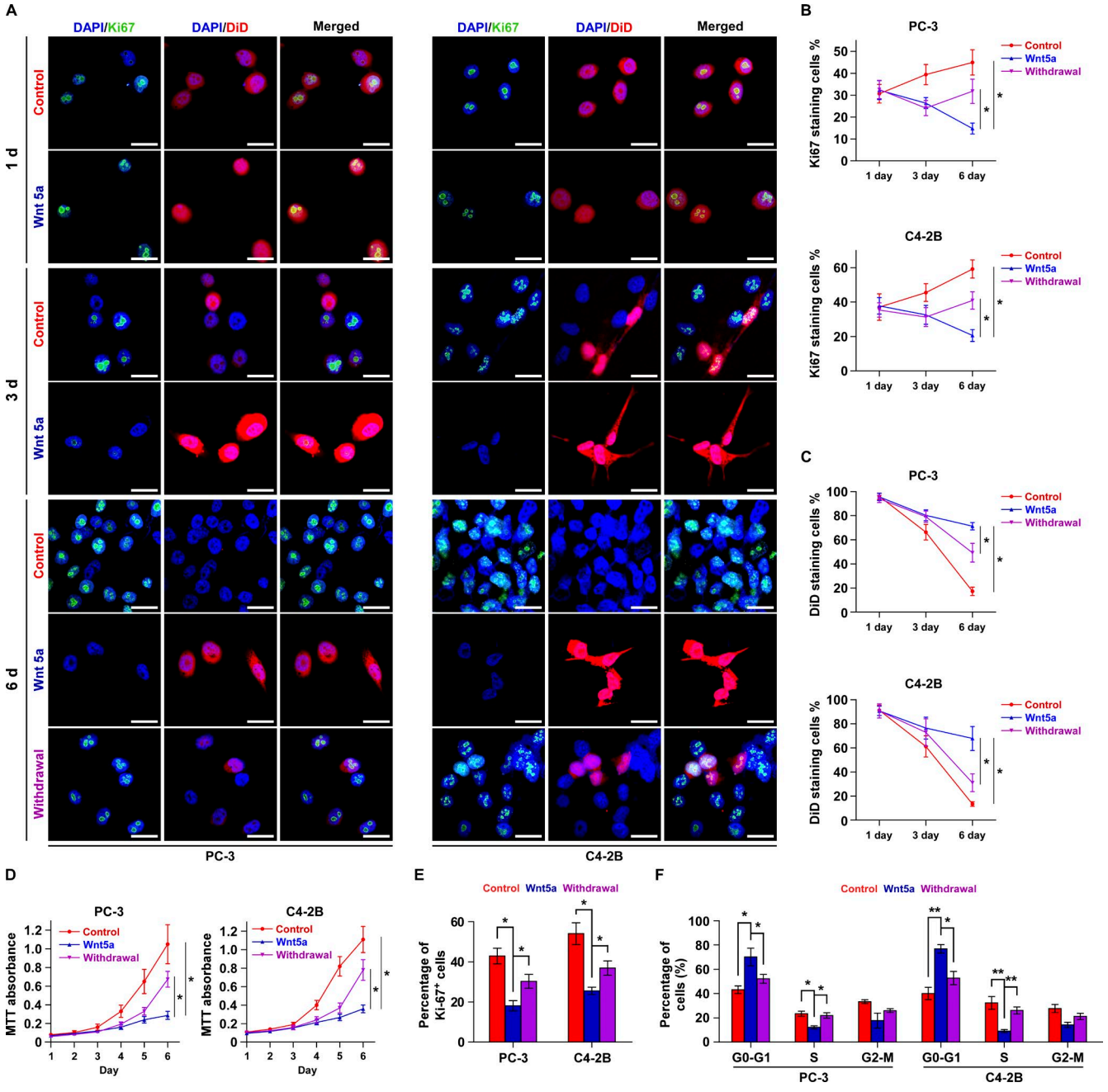

Figure 3. **Wnt5a promoted the dormancy of PCa in a reversible manner in vitro. (A)** Detection of Ki-67–positive (Ki-67$^+$) and DiD-positive (DiD$^+$) cells in untreated (control) or Wnt5a-treated (Wnt5a; 200 ng/ml) PCa cells on days 1 (top), 3 (middle), and 6 (bottom) using immunofluorescence staining. In the withdrawal group, Wnt5a was withdrawn on day 4, and Ki-67$^+$ and DiD$^+$ PCa cells were examined on day 6 (bottom). Bars, 30 µm. **(B and C)** The quantification of Ki-67$^+$ and DiD$^+$ cells in the indicated groups at the indicated time points. Mean ± SD; *, $P < 0.05$ by one-way ANOVA. **(D)** The effect of Wnt5a on proliferation of PCa cells was assessed by MTT assay. Mean ± SD; *, $P < 0.05$ by ANOVA for repeated measures. **(E)** The effects of Wnt5a on the proportion of Ki-67$^+$ cells in the indicated groups on day 5. Mean ± SD; *, $P < 0.05$ by one-way ANOVA. **(F)** The effects of Wnt5a on the cell cycle progression of PCa cells in the indicated groups on day 5. Mean ± SD; *, $P < 0.05$ by one-way ANOVA.

release and can activate several noncanonical Wnt pathways, including protein kinase C (PKC), CaMKII, and NF-AT, all of which can inhibit canonical Wnt/β-catenin signaling via varying mechanisms (Kühl et al., 2000; Saneyoshi et al., 2002; Topol et al., 2003). FACS analysis showed that Wnt5a remarkably increased the influx of Ca^{2+} in PC-3 cells (Fig. S3 A). We further determined which Ca^{2+}-dependent noncanonical Wnt signaling is required for β-catenin decrement by Wnt5a and found that Wnt5a increased the transcriptional activity of NF-AT and p-CaMKII expression, but not p-PKC expression (Fig. S3, B and C). We further treated PC-3 cells with Cyclosporin A (CsA), a specific inhibitor of calcineurin, or KN93, an inhibitor that blocks the binding of calmodulin to the kinase, and found that inhibition of calcineurin or CaMKII activity did not rescue the Wnt/β-catenin activity repressed by Wnt5a (Fig. S3, D and E). Functional experiments revealed that Wnt5a inhibited the number of Ki-67$^+$ cells inde-

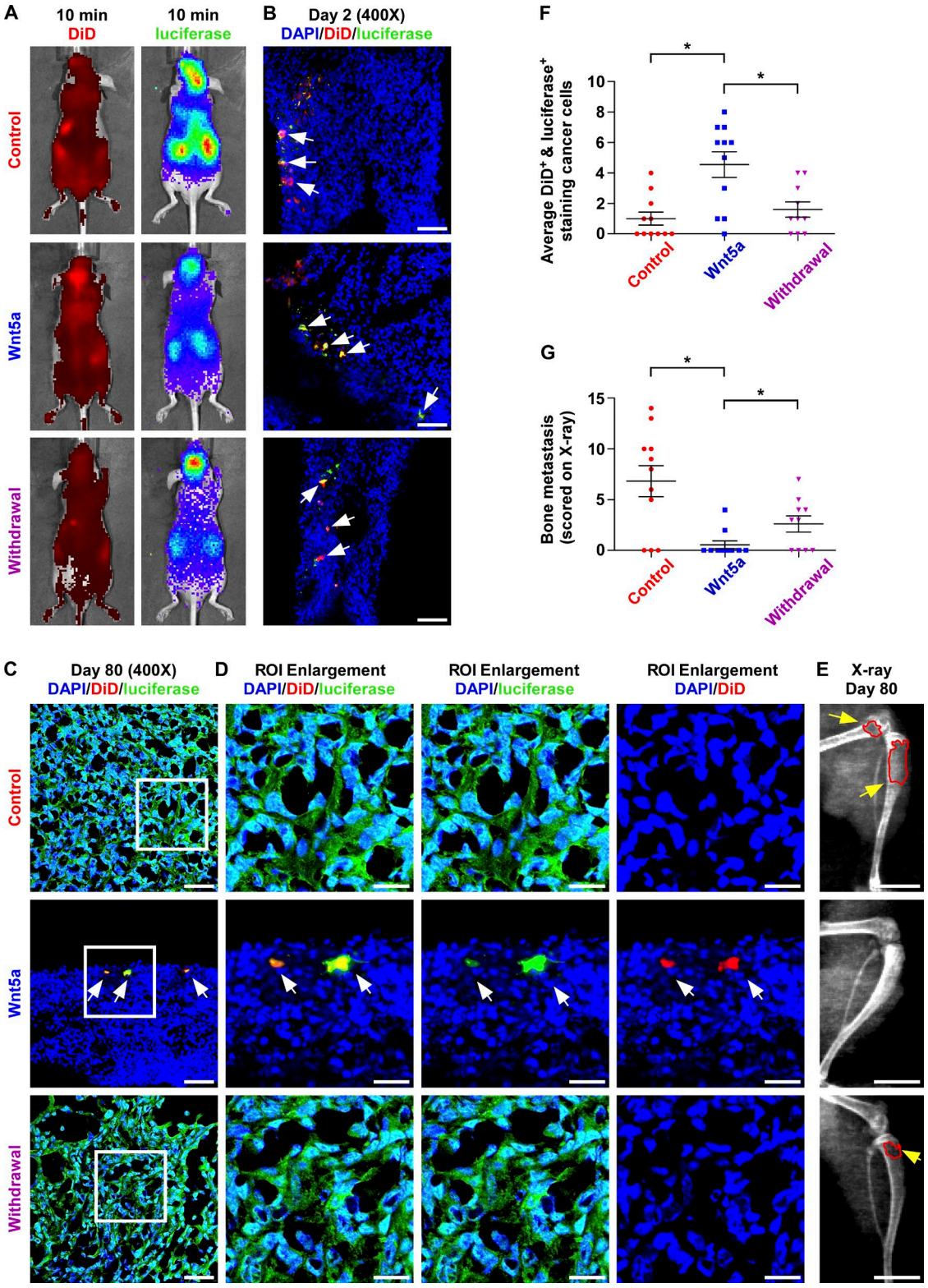

Figure 4. **Wnt5a induced dormancy of PCa cells in vivo in a reversible manner. (A)** Representative images of the control, preWnt5a, and withdrawal mice groups at 10 min. In the withdrawal group, Wnt5a was withdrawn on day 41. **(B)** Images of dormant cell (white arrows) in the indicated mice groups on day 2. Bars, 50 µm. **(C)** Images of dormant cell in the indicated mice groups. Bars, 50 µm. **(D)** The regions of interest (ROI; threefold enlargement) in the white square of C are presented. Bars, 20 µm. **(E)** Representative radiographical images of osteolytic lesions (yellow arrows) in the indicated mice groups. Bars, 4 mm. **(F)** The quantification of double DiD$^+$ and luciferase$^+$ cells in the control (n = 11), Wnt5a (n = 11), and withdrawal (n = 10) groups. Mean ± SEM; *, P < 0.05 by one-way ANOVA. **(G)** The sum of bone metastasis scores in the tibia of the indicated mice groups. Mean ± SEM; *, P < 0.05 by one-way ANOVA.

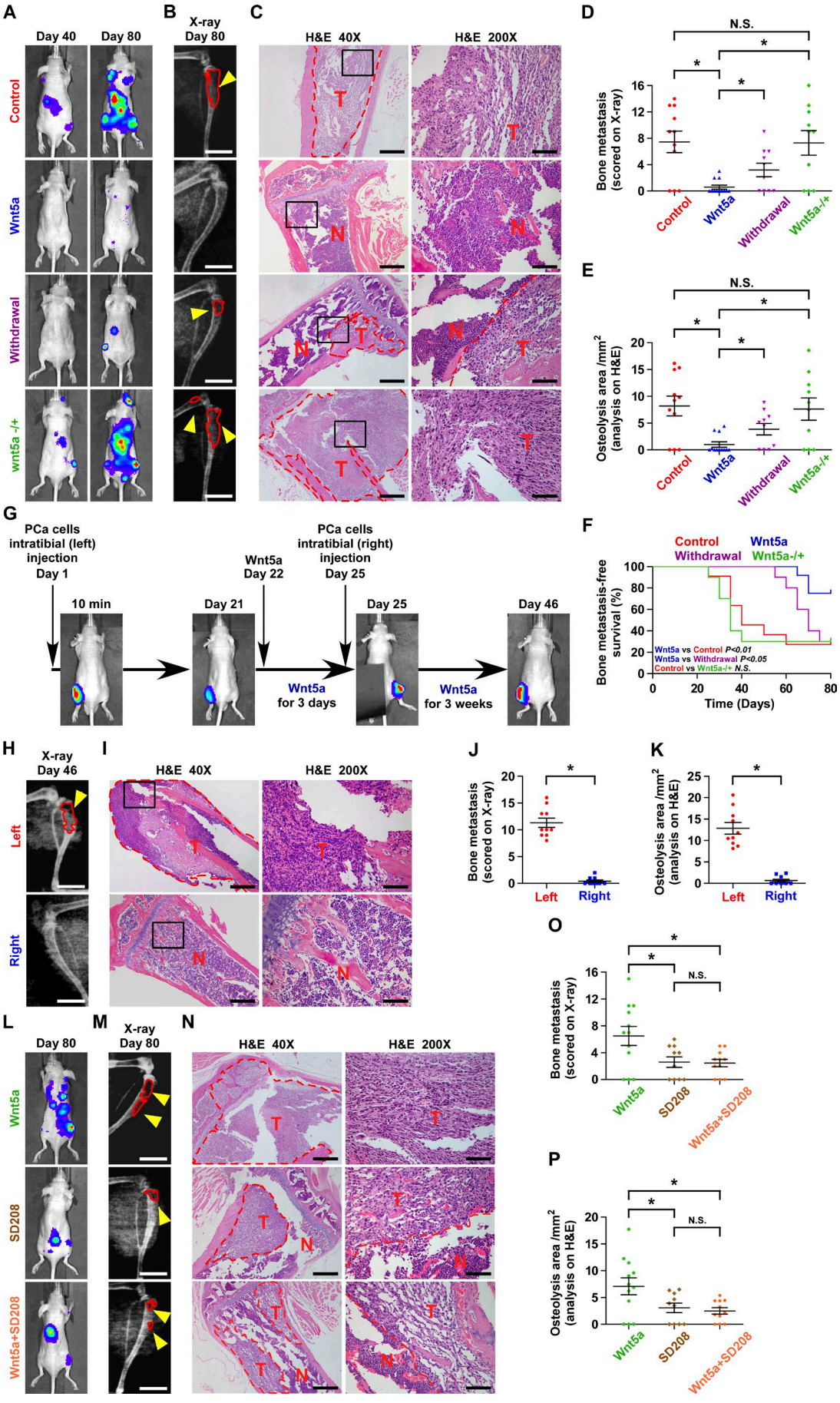

pendent of NF-AT or CaMKII signaling (Fig. S3 F). There results indicate that NF-AT and CaMKII activity are not essential for Wnt5a-induced β-catenin repression and low growth in PCa cells.

Wnt5a inhibits Wnt/β-catenin signaling independent of GSK-3β

As proteasome-mediated degradation of β-catenin has been reported to be a primary mechanism contributing to β-catenin degradation (Klein and Melton, 1996), a proteasome inhibitor, epoxomicin, was used to block proteasome-mediated protein degradation (Meng et al., 1999). As shown in Fig. 7 D, Wnt/β-catenin activity repressed by Wnt5a was obviously inhibited in cells treated with epoxomicin, indicating that Wnt5a inhibits β-catenin via a proteasome-mediated mechanism. As proteasome-mediated degradation of β-catenin phosphorylated by GSK-3β has been reported to be a primary mechanism contributing to β-catenin degradation (Klein and Melton, 1996), we further investigated whether inhibition of canonical Wnt/β-catenin signaling by Wnt5a depends on GSK-3β. As shown in Fig. S3 G, Wnt5a was still able to inhibit Wnt/β-catenin activity in the presence of lithium chloride (LiCl), a specific inhibitor of GSK-3β. Therefore, it is conceivable that Wnt5a is able to decrease the expression of mutant β-catenin, Δβ-catenin, which lacks amino acids 29–48 that contain the GSK-3 phosphorylation sites required for β-catenin degradation (Fig. S3 H; Tetsu and McCormick, 1999). Collectively, these results indicate that inhibition of β-catenin expression by Wnt5a was independent of GSK-3β, as well as suggest that another proteasome-mediated degradation mechanism of β-catenin is involved in β-catenin degradation.

Wnt5a inhibits Wnt/β-catenin signaling via inducing SIAH2

As shown above, Wnt5a induces mutant β-catenin degradation in PC-3 cells, and studies have demonstrated that mutant β-catenin can be targeted for proteasome-mediated degradation through the E3 ubiquitin ligase complex containing SIAH1 or 2, APC, and Ebi, but not GSK-3β or β-TrCP (Liu et al., 2001; Matsuzawa and Reed, 2001). Therefore, we further examined whether SIAH activity is required for Wnt5a-induced β-catenin degradation. As shown in Fig. 7 E, Wnt5a only increased SIAH2 expression. Importantly, a dominant negative SIAH2 (ΔSIAH2) rescued Wnt/β-catenin activity repressed by Wnt5a (Fig. 7 F). As it has been demonstrated that Siah promotes β-catenin degradation requiring Ebi activity (Liu et al., 2001; Matsuzawa and Reed, 2001), the role of Ebi in SIAH2-induced degradation of β-catenin was investigated using Ebi(ΔF), a mutant Ebi lacking the F box domain required for association with Skp1 and β-catenin. As shown in Fig. 7 G, Ebi(ΔF) obviously prevented Wnt5a-induced inhibition of Wnt/β-catenin activity. Meanwhile, ΔSIAH2 or ΔEbi abrogated the roles of Wnt5a in inducing the dormancy of PCa cells in vitro (Fig. S4, A–E) and in vivo (Fig. S4, F–I). Collectively, these results indicate that Wnt5a promotes the degradation of β-catenin by inducing SIAH2 in PCa cells.

ROR2 is essential for Wnt5a-induced dormancy

Wnt5a inhibits Wnt3a-induced Wnt signaling via inducing SIAH2 expression in a ROR2-dependent manner (Mikels and Nusse, 2006). Therefore, we further evaluated whether silencing *ROR2* abrogates Wnt5a-induced dormancy in bone metastasis (Fig. 8, A and B). As shown in Fig. 8 (C and D), silencing *ROR2* reversed the inhibitory effects of Wnt5a on Wnt/β-catenin activity. Importantly, silencing ROR2 reduced the number of DiD^+ cells maintained by Wnt5a in vitro and double DiD^+ and $luciferase^+$ cells in vivo, as well as attenuated the inhibitory effect of Wnt5a on osteolytic bone tumors in vivo (Fig. 8, E–J). Thus, these results indicate that ROR2 is essential for Wnt5a-induced dormancy of PCa cells in bone.

Clinical relevance of Wnt5a/ROR2/SIAH2 signaling in clinical PCa samples

The clinical relevance of the Wnt5a/ROR2/SIAH2 signaling axis were first investigated in a large number of clinical PCa tissues and metastatic bone tissues. As shown in Fig. 9 A and Fig. S5 A, Wnt5a expression in metastatic bone tissues (BM) was significantly higher than that in primary PCa tissues with bone metastasis (PCa/BM) and that in primary PCa tissues without bone metastasis (PCa/nBM), but no significant difference was found between PCa/nBM and PCa/BM. Furthermore, expression of ROR2 and SIAH2 was decreased in PCa/BM and BM compared with those in PCa/nBM, and nuclear β-catenin level was gradually increased in PCa/nBM, PCa/BM, and BM (Fig. 9 A and Fig. S5 A). Of note, there was no significant difference in ROR2 expression between PCa/BM and BM (Fig. 9 A and Fig. S5 A). This finding suggested that low expression of ROR2 may be an early event, which occurred in primary PCa tissues before tumor

Figure 5. **Wnt5a attenuated osteolytic bone tumor tumorigenesis in vivo. (A)** Representative BLI signal of bone metastasis in the indicated mice groups. Wnt5a−/+: Wnt5a was administered on day 41. **(B)** Representative radiographical images of bone metastases in the indicated mice. Bars, 4 mm. **(C)** Representative H&E-stained sections of the tibiae from the indicated mice groups (T, tumor; N, the adjacent nontumor tissues). Bars, 500 µm (40×) and 100 µm (200×). **(D)** The sum of bone metastasis scores in the tibia of the control (n = 11), Wnt5a (n = 12), withdrawal (n = 10), or Wnt5a−/+ (n = 10) mice groups. Mean ± SEM; *, P < 0.05, and N.S. indicates no significance by one-way ANOVA. **(E)** Histomorphometric analysis of bone osteolytic areas in the tibia of the indicated groups. Mean ± SEM; *, P < 0.05, and N.S. indicates no significant by one-way ANOVA. **(F)** Kaplan–Meyer analysis of bone metastasis–free survival in the indicated mice groups. **(G)** The time point, duration, and tibial site of cell or Wnt5a injection were depicted in a schematic model. **(H)** Representative radiographical images of osteolytic bone tumor in the indicated tibia of the mice (n = 10). Bars, 4 mm. **(I)** Representative H&E-stained sections of the indicated tibia of the mice. Bars, 500 µm (40×) and 100 µm (200×). **(J)** The scores of osteolytic bone tumor in the indicated tibia of the mice. Mean ± SEM; *, P < 0.05 by unpaired t test. **(K)** Histomorphometric analysis of bone osteolytic areas in the tibia of the indicated groups. Mean ± SEM; *, P < 0.05 by unpaired t test. **(L)** Representative BLI signal of bone metastasis in the mice treated with Wnt5a (50 µg/kg; n = 12), SD208 (50 mg/kg/d; n = 10), or Wnt5a + SD208 (n = 11). **(M)** Representative radiographical images of bone metastases in the indicated mice. Bars, 4 mm. **(N)** Representative H&E-stained sections of the tibiae from the indicated mice. Bars, 500 µm (40×) and 100 µm (200×). **(O)** The sum of bone metastasis scores in the tibia of the indicated mice groups. Mean ± SEM; *, P < 0.05, and N.S. indicates no significance by one-way ANOVA. **(P)** Histomorphometric analysis of bone osteolytic areas in the tibia of the indicated mice groups. Mean ± SEM; *, P < 0.05, and N.S. indicates no significance by one-way ANOVA.

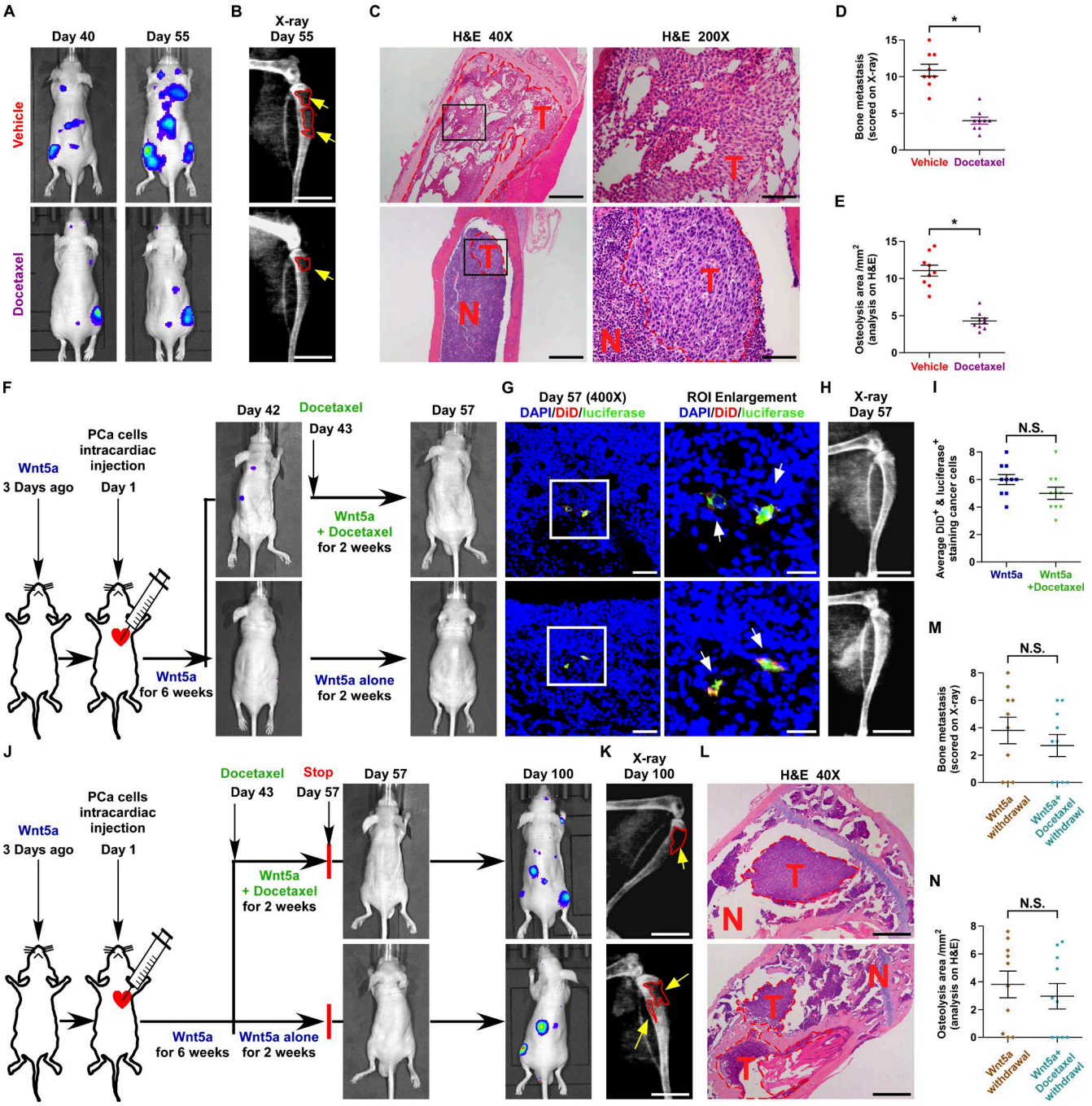

Figure 6. **Dormant PCa cells induced by Wnt5a exhibited resistance to docetaxel in vivo. (A)** Representative BLI signal of bone metastasis in the vehicle (0.9% NaCl solution; $n = 9$) or docetaxel-treated mice groups ($n = 9$). **(B)** Representative radiographical images of osteolytic bone tumors in the indicated mice. Bars, 4 mm. **(C)** Representative H&E-stained sections of tibiae in the indicated groups (T, tumor; N, the adjacent nontumor tissues). Bars, 500 µm (40×) and 100 µm (200×). **(D)** The sum of bone metastasis scores in the tibiae of the indicated groups. Mean ± SEM; *, $P < 0.05$ by unpaired *t* test. **(E)** Histomorphometric analysis of bone osteolytic areas in the tibiae of the indicated mice groups. Mean ± SEM; *, $P < 0.05$ by unpaired *t* test. **(F)** A schematic model illustrated time points and duration of Wnt5a ($n = 10$) or docetaxel ($n = 10$) administration. **(G)** Confocal microscope of tibiae in the indicated groups. Bars, 50 µm (400×) and 20 µm (ROI). **(H)** Representative radiographical images of osteolytic bone tumors in the indicated groups. Scale bar, 4 mm. **(I)** The quantification of double DiD⁺ and luciferase⁺ cells in the indicated groups. Mean ± SEM indicates no significance by unpaired *t* test. **(J)** A schematic model illustrated the time points and duration of administration or removal of Wnt5a or docetaxel. **(K)** Representative radiographical images of osteolytic bone tumors in the indicated mice. Bars, 4 mm. **(L)** Representative H&E-stained sections of tibiae from the indicated mice. Bars, 500 µm. **(M)** The sum of bone metastasis scores in the tibiae of the mice groups of removing Wnt5a + docetaxel ($n = 10$) or Wnt5a alone ($n = 10$). Mean ± SEM indicates no significance by unpaired *t* test. **(N)** Histomorphometric analysis of bone osteolytic areas in the tibia of the indicated mice groups. Mean ± SEM. N.S. indicates no significance by unpaired *t* test.

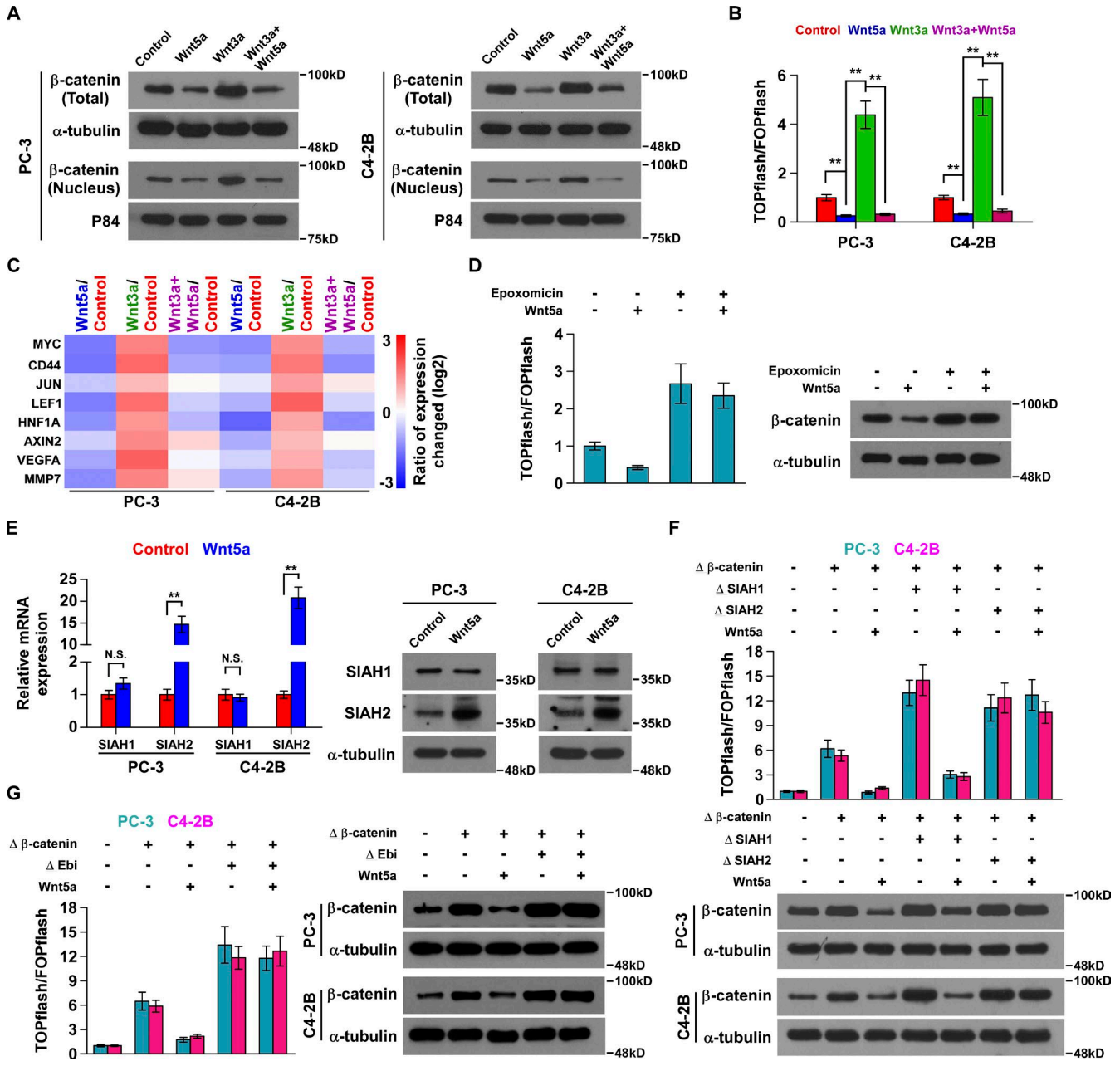

Figure 7. **Wnt5a inhibited canonical Wnt/β-catenin signaling via inducing SIAH2 expression. (A)** Total and nuclear expression of β-catenin in the indicated PC-3 cells. α-Tubulin and p84 were used as total and nuclear loading controls, respectively. The experiment was independently performed three times. **(B)** The TOP/FLASH reporter activity in the indicated PC-3 cells. Mean ± SD; **, P < 0.01 by one-way ANOVA. **(C)** Real-time PCR results of the multiple downstream target genes of β-catenin signaling in the indicated PC-3 cells. Pseudo-color scale values were log2 transformed. Transcript levels were normalized by GAPDH expression. The experiment was independently performed three times. **(D)** The effects of epoxomicin (100 nM; 8 h) on TOP/FLASH reporter activity and endogenous β-catenin expression. α-Tubulin served as the loading control. Mean ± SD. **(E)** Real-time PCR and Western blot analysis of SIAH1 and SIAH2 mRNA and protein expression in Wnt5a-treated PCa cells (200 ng/ml). Transcript levels were normalized to GAPDH. α-Tubulin served as the loading control. Mean ± SD; *, P < 0.05, and N.S. means no significance by unpaired *t* test. **(F)** Western analysis of the effect of ΔSIAH2 on TOP/FLASH activity and β-catenin expression in the indicate cells. α-Tubulin was used as the loading control. Mean ± SD. **(G)** Western analysis of the effect of ΔEbi on TOP/FLASH activity and β-catenin expression in the indicate cells. α-Tubulin was used as the loading control. Mean ± SD.

cells arrive in the bone. Statistical analysis revealed that nuclear β-catenin level was positively correlated with bone metastasis status and poor bone metastasis–free survival in PCa patients, but ROR2 expression was inversely correlated this, whereas SIAH2 and Wnt5a expression had no significant association with bone metastasis–free survival in PCa patients (Fig. 9, B and C; and Fig. S5, B and C). Notably, although ROR2 and SIAH2 expression were found to be up-regulated in PCa/nBM, compared with those in PCa/BM, and overexpression of ROR2 and SIAH2 were significantly correlated with bone metastasis status (Fig. 9, A and B; and Fig. S5, A and B), only ROR2 expression was significantly and strongly associated with bone metastasis–free

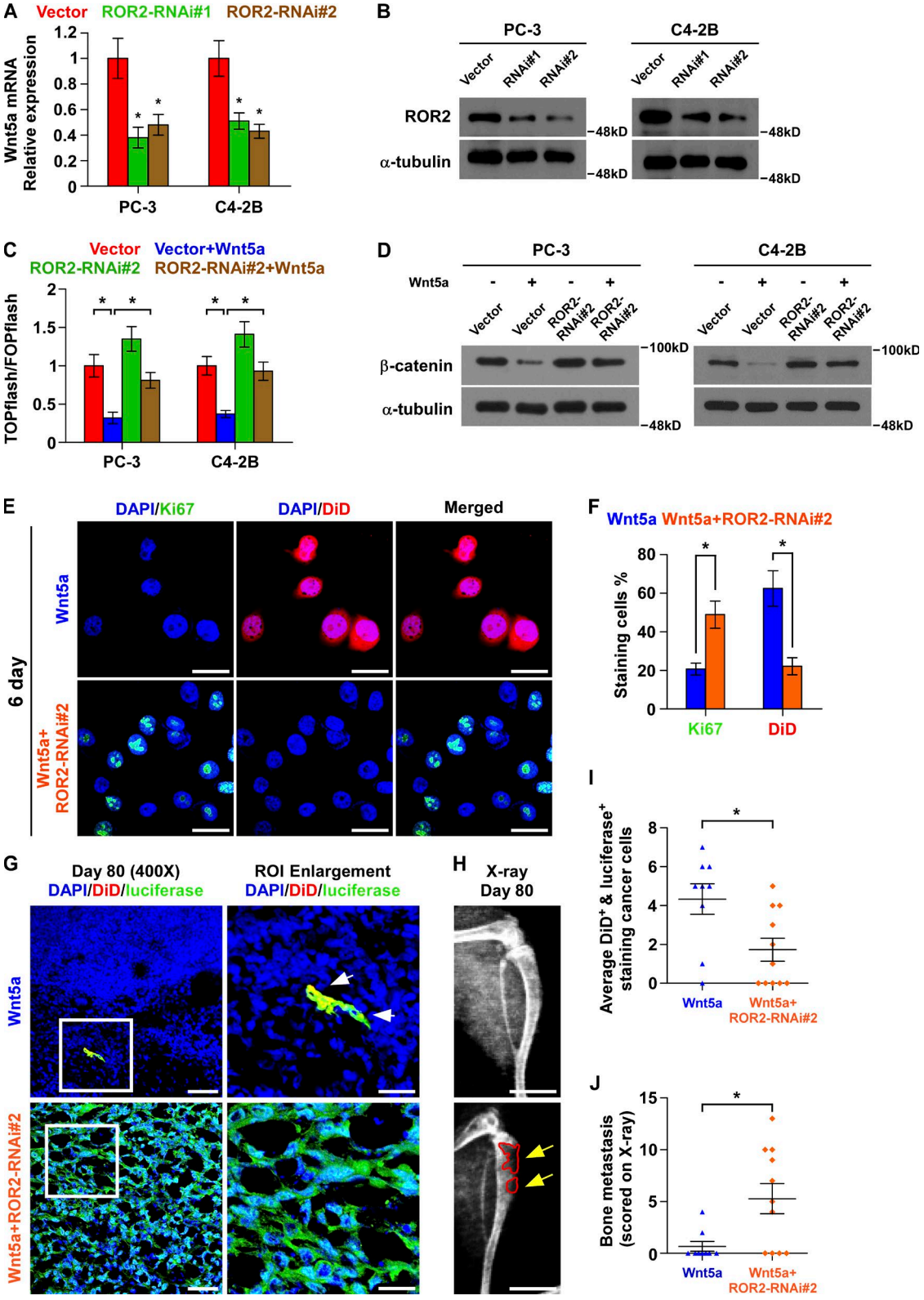

Figure 8. **ROR2 was essential for Wnt5a-induced dormancy. (A and B)** Real-time PCR and Western blot analysis of ROR2 expression in the indicated PCa cells. Transcript levels were normalized by GAPDH expression. α-Tubulin served as the loading control. Mean ± SD; *, P < 0.05 by one-way ANOVA. **(C and D)** The effect of ROR2 silencing on TOP/FLASH reporter activity and endogenous β-catenin expression. Transcript levels were normalized to GAPDH. α-Tubulin served as the loading control. Mean ± SD; *, P < 0.05 by one-way ANOVA. **(E)** Immunofluorescent staining of Ki-67 and DiD in the indicated cells. Bars, 30 µm. **(F)** The quantification of Ki-67$^+$ and DiD$^+$ cell number in the indicated groups. Mean ± SD; *, P < 0.05 by unpaired *t* test. **(G)** Confocal microscope of tibiae in the indicated mice groups. Bars, 50 µm (400×) and 20 µm (ROI). **(H)** Representative radiographical images of bone metastases in the indicated mice. Bars, 4 mm. **(I)** The quantification of double DiD$^+$ and luciferase$^+$ cells in the indicated mice groups. Mean ± SEM; *, P < 0.05 by unpaired *t* test. **(J)** The sum of bone metastasis scores in the tibia of the Wnt5a treatment (n = 9) and Wnt5a treatment + ROR2-silenced (n = 11) mice groups. Mean ± SEM *, P < 0.05 by unpaired *t* test.

survival in PCa patients (Fig. 9 C). This may be explained by the possibility that the Wnt5a level secreted by primary PCa cells might be not enough to dramatically activate ROR2/SIAH2 signaling compared with that in the osteoblastic niche, suggesting that the Wnt5a/ROR2/SIAH2 axis plays a more important role in inducing dormancy of PCa cells in bone microenvironment than that in the primary PCa microenvironment. Meanwhile, our findings also indicate that ROR2 could be used be as a reliable biomarker in predicting bone metastasis in PCa patients compared with SIAH2 or Wnt5a. Importantly, we found that BM with low levels of ROR2 and SIAH2 exhibited high nuclear β-catenin level (Fig. 9 A), indicating that reduced ROR2 disrupts Wnt5a/SIAH2 signaling, which results in activation of canonical Wnt/β-catenin signaling, consequently promoting the development of osteolytic tumors in bone.

To further determine the clinical significance of Wnt5a/ROR2/SIAH2 signaling axis, primary PCa cells recovered from clinical PCa tissues were first isolated. Only the tissues with <15% of contaminating benign cells by H&E staining were used for the establishment of primary PCa cells (Fig. S5 D). After isolation, primary PCa cells were generated by co-culturing with the feeder cells (irradiated 3T3 mouse fibroblasts) in the presence of a Rho-associated protein kinase inhibitor (Fig. S5, E and F), and further evaluated via examining expression of several prostate-associated or epithelial proteins (Fig. S5 G). To evaluate Wnt5a/ROR2/SIAH2 signaling pathway in primary PCa cells, ROR2 expression was first examined. As shown in Fig. 9 D, ROR2 expression was detectable in three of four primary PCa cells. We further treated the primary PCa cells with Wnt5a and found that Wnt5a differentially up-regulated SIAH2 expression and reduced β-catenin expression in three independent primary PCa cells that expressed relatively higher levels of ROR2 (Fig. 9 E). Therefore, our results provide clinical evidence that Wnt5a could activate ROR2/SIAH2 signaling in primary PCa cells isolated from clinical PCa samples. Collectively, our results indicate that Wnt5a from osteoblastic niche suppresses canonical Wnt/β-catenin signaling dependent on SIAH2/ROR2 signaling, which ultimately induces dormancy of PCa cells in bone (Fig. 9 F).

Discussion

The dormant state of metastatic cells is under precise control of microenvironment within the metastasized organs (Aguirre-Ghiso, 2007). Several secretory factors from the tumor microenvironment play important roles in the induction of cancer cell dormancy (Kobayashi et al., 2011; Jung et al., 2016). After arrival in bone under CXCR4/CXCR12 signaling, tumor cells compete with HSCs and finally colonize in the location previously occupied by HSCs in the osteoblastic niche (Shiozawa et al., 2011; Lawson et al., 2015). Importantly, Wnt5a maintains HSCs in a quiescent G_0 state (Nemeth et al., 2007), suggesting that Wnt5a may be implicated in the cell dormancy. Here, our results demonstrated that Wnt5a from osteoblastic niche contributed to the dormancy of PCa cells in bone. This finding, in combination with other studies (Kobayashi et al., 2011; Jung et al., 2016), elucidates the critical roles of tumor microenvironment in induction and maintenance of cell dormancy.

Osteoblastic niche is a highly Wnt5a-containing compartment in the physiological condition (Maeda et al., 2012; Sugimura et al., 2012). Importantly, Wnt5a has been reported to maintain HSCs in a quiescent G_0 state (Nemeth et al., 2007). Therefore, it is conceivable that arrival of PCa cells into the osteoblastic niche confronts a microenvironment with high levels of Wnt5a and is prone to enter a dormant state within the niche, as demonstrated by our results that systemic administration of Wnt5a that repressed canonical Wnt/β-catenin signaling via activation of ROR2/SIAH2 signaling maintained the dormant state of PCa cells in vivo. In fact, suppression of Wnt/β-catenin signaling has been demonstrated to be an early event to maintain and induce metastatic dormancy of cancer cells (Malladi et al., 2016), which further supports our findings. Strikingly, Wnt5a expression is significantly decreased in aged mice (Rauner et al., 2008). These findings may partially explain that the appearance of metastatic bone tumors after several years of PCa diagnosis may be associated with a loss of Wnt5a with aging. However, further studies are necessary to confirm this hypothesis.

Wnt5a not only plays critical roles in a myriad of developmental processes (Yamaguchi et al., 1999; Nishita et al., 2010), but is also implicated in multiple human malignancies (Kremenevskaja et al., 2005; Takiguchi et al., 2016). Compared with the relatively explicit role of Wnt5a in breast cancer (tumor suppressor; Jönsson et al., 2002; Cai et al., 2013) and melanoma (tumor promotor; Weeraratna et al., 2002; Da Forno et al., 2008), its role in PCa remains ambiguous (Yamamoto et al., 2010; Syed Khaja et al., 2011; Takahashi et al., 2011; Thiele et al., 2015). Controversial roles of Wnt5a in cancer may be explained by the study from Mikels and Nusse that receptor context governed Wnt signaling output; namely, signaling initiated by Wnt5 is not intrinsically regulated by Wnt5a itself but by receptor availability, which may produce totally different biological roles even in the same type of cancer (Mikels and Nusse, 2006). Indeed, overexpression of Wnt5a enhanced invasion activity of PCa cells, which required FZD2 and ROR2 as Wnt receptors (Yamamoto et al., 2010); moreover, Thiele reported that Wnt5a functioned as a tumor suppressor via binding to FZD5 (Thiele et al., 2015). In this study, we found that the inducible role of Wnt5a in dormancy of PCa cells is dependent on ROR2 expression. Through immunohistochemical (IHC) analysis in PCa tissues, we found that ROR2 expression was dramatically down-regulated in PCa/BM, compared with PCa/nBM, but there was no significant difference compared with BM. Importantly, ROR2 expression negatively correlated with poor bone metastasis–free survival in PCa patients. This finding indicated that ROR2 expression was already reduced in primary PCa tissues before implanting in bone; namely, the expression level of ROR2 in primary PCa tissues may determine the fate of PCa cells colonized in bone. As the samples of metastatic bone tissues analyzed in this study were limited, a more solid conclusion will be warranted in a larger series of studies.

The previous study has demonstrated that increased Wnt5a in PC-3 cells dramatically reduced the tumor burden in bone (Thiele et al., 2015). Consistently, systemic administration of Wnt5a induced the dormancy of PCa cells in bone and meanwhile inhibited the formation of metastatic bone tumor in vivo in a preventive protocol. However, injection of Wnt5a at week 7

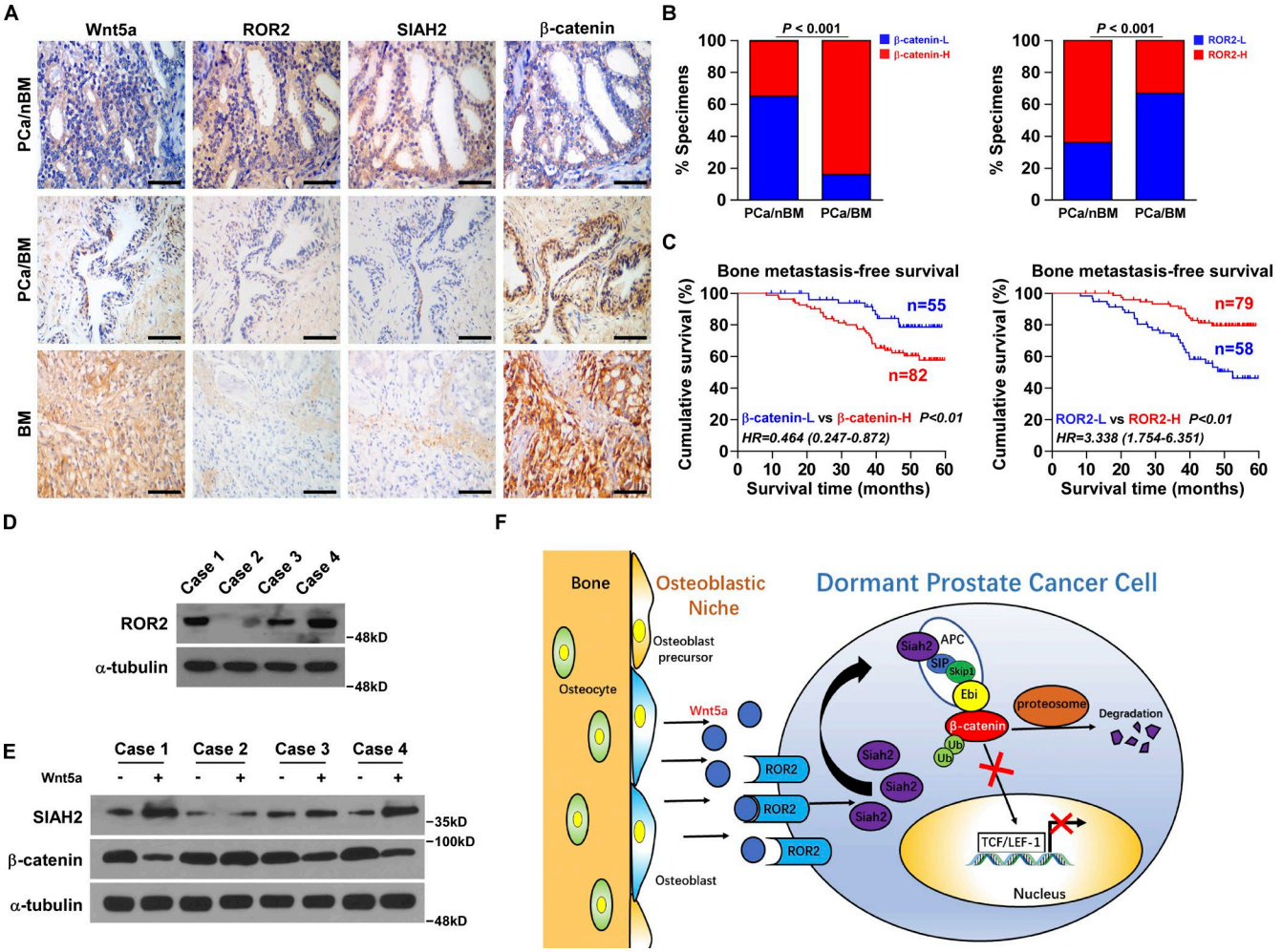

Figure 9. **Clinical relevance of Wnt5a/ROR2/SIAH2 signaling in clinical PCa samples. (A and B)** IHC staining of Wnt5a, ROR2, SIAH2, and nuclear β-catenin expression in representative samples of PCa tissues without bone metastasis (PCa/nBM; *n* = 134), PCa tissues with bone metastasis (PCa/BM; *n* = 97), and metastatic bone tissues (BM; *n* = 11) were shown. Bars, 50 µm. **(B)** Percentage of samples showing low or high expression levels of ROR2 or nuclear β-catenin intensity in PCa/nBM or PCa/BM tissues. P < 0.001 by χ^2 test. **(C)** Kaplan–Meier analysis of bone metastasis–free survival curves in PCa patients with low ROR2 or nuclear β-catenin expression versus high ROR2 or nuclear β-catenin expression. **(D)** Western blotting analysis of ROR2 expression in primary PCa cells. α-Tubulin served as the loading control. The experiment was independently performed three times. **(E)** Expression of SIAH2 and β-catenin in response to Wnt5a (200 ng/ml) treatment in primary PCa cells. α-Tubulin was used as the loading controls. The experiment was independently performed three times. **(F)** Schematic model for Wnt5a-induced dormancy of PCa cells in bone.

did not reduce the tumor burden. Indeed, Malladi et al. (2016) stated that Wnt activation is an early event in the eventual outgrowth of metastatic lesions. This paradoxical effect of Wnt5a on bone metastasis of PCa may be associated with the "vicious cycle" that gave rise to the net results of Wnt5a administration showing no significant difference, compared with the control groups, after the bone tumor formed. Our results further demonstrated that administration of Wnt5a with SD208 significantly reduced the osteolytic area compared with Wnt5a treatment alone. However, Wnt5a + SD208 did not exhibit more efficacy than SD208 alone. Therefore, our results provide evidence that in PCa patients without metastatic bone tumors at the onset of diagnosis, administration of Wnt5a might be useful as a prophylactic avenue to maintain tumor cells indefinitely in a dormant state. However, for those PCa patients with metastatic bone tumors at first diagnosis, Wnt5a does not show significant efficacy on osteolytic bone tumors, even in combination with SD208, suggesting that Wnt5a inhibits the bone metastasis of PCa in a preventive manner.

A cure for bone metastasis cannot be achieved until the fundamental drivers of bone metastasis, particularly the drivers for cells survival during dormancy or exit from this state, are discovered (Esposito et al., 2018). This study is the first, to the best of our knowledge, to investigate of the role of Wnt5a in vivo and demonstrate the inducible role of Wnt5a in the dormancy of tumor cells in bone. Increasing interest in cancer dormancy has primarily lied in metastatic behavior of cancer, which contributes to the vast majority of cancer-related deaths (Pantel and Brakenhoff, 2004). In this scenario, the existence of dormant disseminated cells has been recognized in cancer patients in whom dormancy renders tumor cells resistant to anti-tumor therapies, which has been demonstrated by our and other studies (Essers and Trumpp, 2010; Ebinger et al., 2016). Once the dormant state is disrupted, cells will proliferate unlimitedly, resulting in the

decline of patient survival. Thus, exploration of the molecular target that maintains tumor cell dormancy, such as Wnt5a identified in this study, will be beneficial for patient survival. In fact, the potential that Wnt5a may be used in the clinic presents a promising prospect, because Wnt5a has been used as an efficient and safe therapeutic method in Parkinsonian mice (Parish et al., 2008) and even in the metastatic spread of PCa in an orthotopic mouse model (Canesin et al., 2017).

Limitations of our study should be noticed when interpreting and extrapolating our data. Wnt5a should be tested in other osteotropic cancer entities. Additionally, a more ideal model system should be used if possible, preferably an intraprostatic injection mouse model. Finally, the functional domain of Wnt5a needs to be further identified.

In summary, a new approach to confine cancer cells in the state of perpetual dormancy is presented in our study. Activation of SIAH2/ROR2 signaling by Wnt5a induces the dormancy of PCa cells and prevents the formation of metastatic bone tumor. Therefore, it is likely that Wnt5a will be an optimal anti-bone metastatic strategy for PCa patients, especially the ones without bone metastasis at first diagnosis, in the future.

Materials and methods

Cell culture

The human PCa cell lines PC-3 derived from metastatic bone site, mouse preosteoblastic cell line MC3T3-E1, and human osteoblast cells (hFOB1.19) were obtained from the Shanghai Chinese Academy of Sciences cell bank (Shanghai, China). PC-3 was cultured in RPMI-1640 medium (c11875500bt; GIBCO) supplemented with 10% FBS (10099-141; GIBCO), MC3T3-E1 in Alpha Minimum Essential Medium (A1049001; GIBCO), and hFOB1.19 in F-12 medium (12400024; GIBCO). The LNCaP-derived bone metastatic cell line C4-2B was purchased from MD Anderson Cancer Center and maintained in T-medium (A1048501; GIBCO) supplemented with 10% FBS (Wu et al., 1998). BMSCs were purchased from ATCC and cultured according to the ATCC protocol. All cell lines were grown under a humidified atmosphere of 5% CO_2 at 37°C, except for hFOB1.19 at 33.5°C. For the transwell co-culture model, different densities of PCa cells were seeded on the lower chamber of 6-well plate according to the requirements of different assays, and the culture insert with 0.4-µm pore size (3412; Corning) was placed on the top of each well followed by seeding with 5×10^5 osteoblasts in the upper chamber of transwell.

Isolation and culture of primary osteoblasts and associated assays

Primary osteoblasts were obtained from the calvaria of neonatal rats (2–3 d old). The detailed procedures were performed as follows: five neonatal rats were sacrificed and sterilized with 75% ethanol two times; the cadaver of the rat was placed in a large Petri dish; the head was removed using large scissors; the head was grasped at the nape of the neck, and a small incision was made along the base of the skull (small scissors make the cleanest cut); the skin and the brain tissue were carefully removed from the skull using a scalpel and tweezer; the jaw was cut away, and any excess tissue and cartilage were scraped off from around the edge of the calvaria; the calvaria was cut in half, placed in a 15-ml conical base centrifuge tube, and washed with 1× PBS three times; the calvaria was incubated in 1% trypsin (1 ml/calvarial bone) for 10 min at 37°C and removed, and the trypsin solution was discarded and washed in supplemented DMEM (sDMEM) two times (serum and calcium in the medium will inactivate any residual trypsin), incubated in 0.2% collagenase solution (800 µl/calvarial bone) for 30 min at 37°C, and then the collagenase digest was removed and discarded and then replaced with fresh collagenase solution for a further 60 min at 37°C; the final digest was kept and transferred to a 15-ml conical base centrifuge tube; calvaria was washed with sDMEM (5 ml) two times, and the solution was transferred to the 15-ml tube containing the final digest; the cell solution was spun at 1,500 *g* for 5 min at room temperature, the supernatant was discarded, and the cell pellet was resuspended in sDMEM (1 ml/calvarial bone); the cell suspensions were transferred to 2 × 75–cm^2 flask, and then 20 ml of sDMEM and 1 ml of cell suspension were added to the flask; the flask was incubated under a humidified atmosphere of 5% CO_2 at 37°C until the cells reached 80∼90% confluency (∼3 d) for use.

Bone formation assay was performed in 24-well tissue culture trays at a density of 2.5×10^4 cells/well in osteogenesis DMEM, and the cell number was counted using a hemocytometer. Half of the medium was exchanged every 2–3 d. The cell layers of osteoblast were observed by phase contrast microscopy on days 1, 3, 7, and 14, respectively. For alizarin red and alkaline phosphatase (ALP) staining, the cell layers were carefully washed with PBS and then trypsinized, and the cells were transferred to 2.5% glutaraldehyde fixative for 5 min, washed three times with 70% ethanol, and left to air dry; alizarin red (a5533; Sigma) staining for 5 min was followed by three washes with 50% ethanol and left to air dry; ALP (D001-2; Jiancheng BioTech) staining was performed for ∼30 min in the dark; primary osteoblasts were washed with dH_2O and left to air dry. For May-Grunwald and Giemsa (MGG) staining, the cell layers were washed with PBS after proliferating to 80–90% confluence, May-Grunwald (63590; Sigma) staining was performed for 10 min, and Giemsa (Sigma; 48900) staining was performed for 20 min, followed by three washes with 50% ethanol and left to air dry. Osteoblast were stained with ALP and MGG on day 3 and alizarin red on day 21 to demonstrate calcium.

sDMEM, osteogenesis DMEM, collagenase solution, 2.5% glutaraldehyde fixative, and alizarin red and ALP staining buffer were prepared as previously described (Orriss et al., 2012).

Patients, tissue processing, and establishment and characterization of primary PCa cells

Patient consent and approval from the Institutional Research Ethics Committee from The First Affiliated Hospital of Sun Yat-sen University were obtained before the use of these clinical materials for research purposes, and the approval number was [2014]A-011. A total of 231 paraffin-embedded, archived PCa tissues, including 97 primary PCa tissues with bone metastasis and 134 PCa tissues without bone metastasis, and 11 metastatic bone tissues were obtained during surgery or needle biopsy between January 2012 and May 2017 and were diagnosed based on clinical and pathological evidence. The clinicopathological features of the 231 PCa patients are summarized in Table S1.

A total of 17 fresh PCa tissues were collected via radical prostatectomy between May and June 2018. Then, a cylinder shaped core of prostate tissue (8-mm diameter) was cored out of the section of PCa tissue that was determined by an experienced pathologist, based on the appearance of PCa tissues. The cored PCa tissues were then bisected: one half was used to evaluate the ratio of benign and malignant cells in the parental tissue of PCa using H&E staining; the other half of the PCa tissues were frozen at this stage. Only the tissues with <15% of contaminating benign cells by H&E staining were used for the establishment of primary PCa cells. According to this criterion, only six PCa tissues were available for isolation of primary PCa cells. The tissues were first mechanically and enzymatically dissociated. Once the primary PCa cells were isolated from the PCa tissues with collagenase treatment, they were co-cultured with irradiated Swiss 3T3 J2 mouse fibroblasts feeder cells (J2 strain) in F-medium (3:1 [vol/vol] F-12 Nutrient Mixture [Ham]: DMEM [Invitrogen], 5% FBS, 0.4 µg/ml hydrocortisone, 5 µg/ml insulin, 8.4 ng/ml cholera toxin, 10 ng/ml EGF, and 24 µg/ml adenine) supplemented with 10 µM Rho-associated protein kinase inhibitor (Y-27632; Enzo Life Sciences) until the experiments. Differential trypsinization was used to separate the feeder cells from the primary PCa cells during passaging and seeding of the primary PCa cells. Primary PCa cells were successfully generated in four out of six candidate PCa tissues.

RNA extraction, reverse transcription, and real-time PCR

Total RNA from cells was extracted using the TRIzol reagent (Invitrogen) according to the manufacturer's instruction. The extracted RNA was pretreated with RNase-free DNase, and 2 µg of RNA from each sample was used for cDNA synthesis, primed with random hexamers. cDNA was amplified and quantified using a CFX 96 real-time system (Bio-Rad) with iQ SYBR green (Takara) according to the manufacturer's instructions. Expression levels of various genes were normalized to housekeeping gene GAPDH as controls. The sequences of each primer were provided below. Gene expression data were analyzed using the comparative Ct method ($2^{-\Delta\Delta Ct}$).

Luciferase assay

Cells were plated in 24-well plates, proliferating to 60–80% confluence after 24 h of culture, and the reporter plasmids plus 1 ng pRL-TK *Renilla* plasmid (E2241; Promega; original cloned from the marine organism *Renilla reniformis*) were transfected into cells using Lipofectamine 3000 (Life Technologies). 48 h after transfection, the transfection medium was replaced with fresh RPMI-1640 medium; cells were harvested and washed with PBS and lysed with passive lysis buffer (Promega). The cell lysates were analyzed immediately using Synergy 2 microplate system (BioTek). Luciferase and *Renilla* luciferase were measured using a Dual-Luciferase Reporter Assay System (Promega) according to the manufacturer's instructions. The luciferase activity of each lysate was normalized to *Renilla* luciferase activity.

Western blot

Cells were lysed in radioimmunoprecipitation buffer (50 mM Tris, pH 7.4, 1% TX-100, 0.2% Na deoxycholic acid, and 0.2% SDS, HALT complete tab; Roche). Proteins were quantified using the Pierce BCA Protein Assay kit (Thermo Fisher Scientific). Equal amounts of protein were loaded per lane and resolved by SDS-polyacrylamide electrophoresis. Proteins were transferred by semi-dry electrophoresis (Bio-Rad) onto polyvinylidene fluoride (Millipore) and blocked by 5% nonfat milk for 1 h at room temperature. Membranes were incubated overnight at 4°C with anti-cyclin D1, cyclin E1 (Cyclin Antibody Sampler kit; 9869), p21 (2947), p27 (3686), p-CaMKII (12716), p-PKC (9375; Cell Signaling Technology), β-catenin (66379), CK8 (17514-1-AP), CK18 (10830-1-AP), and PSA (10679-1-AP; Proteintech), SIAH1 (SAB1404370), SIAH2 (S 7945), ROR2 (SAB1412202), and AR (5153; Sigma) or p84 (ab102684; Abcam). Membranes were washed thrice (10 min each) in Tis-HCl buffered saline-tween and incubated for 40 min at room temperature with horseradish peroxidase–conjugated anti-mouse or anti-rabbit secondary antibodies (GE Healthcare). Membranes were washed thrice (10 min each) in Tris-HCl–buffered saline-tween and developed on film with the electrochemiluminescence system. The membranes were stripped and reprobed with an anti–α-tubulin antibody (2125; Cell Signaling Technology) as the loading control. Nuclear/cytoplasmic fractionation was separated using the Cell Fractionation kit (Cell Signaling Technology) according to the manufacturer's instructions.

MTT assay

Cells were seeded into 96-well plates in triplicate at the initial density of 0.2×10^4 cells/well, and Wnt5a was added every 12 h for 6 d. At various time points, groups of cells were incubated with 100 µl of 0.5 mg/ml sterile MTT (3-[4, 5-dimethyl-2-thiazolyl]-2, 5-diphenyl-2H-tetrazolium bromide; Sigma) for 4 h at 37°C. The culture medium was then removed, and 150 µl of DMSO (Sigma) was added. The absorbance values were measured at 570 nm, using 655 nm as the reference wavelength.

Cell cycle analysis

After co-culture with osteoblasts in a transwell plate, cultured in the conditioned medium or Wnt5a treatment, cell cycle analysis were performed using Cell Cycle Detection kit (KeyGEN) according to the manufacturer's instructions. PCa cells were harvested by trypsinization, washed in ice-cold PBS and fixed in 75% ice-cold ethanol in PBS. Before staining, cells were gently resuspended in cold PBS, and ribonuclease was added into cells' suspension tube, incubated at 37°C for 30 min, followed by incubation with propidium iodide for 20 min at room temperature. Cell samples were then analyzed by FACSCanto II flow cytometer (Becton, Dickinson, and Company), and the data were analyzed using FlowJo 7.6 software (TreeStar Inc.).

ELISA

Wnt5a, Wnt5b, Wnt11, and Wnt16 were measured by Wnt5a (CSB-EL026138), Wnt5b (CSB-EL026139), Wnt11 (CSB-EL026131), and Wnt16 (CSB-EL026132) ELISA kits (CUSABIO) following the manufacturer's instruction, respectively.

FACS analysis

After co-culture with osteoblasts in a transwell plate, cultured in the conditioned medium or Wnt5a treatment, PCa cells were

stained with mouse anti-human FITC-conjugated Ki-67 and 7-AAD (BD Biosciences). G_0/G_1 cells were gated and analyzed for the percentage of cells that were in the G_0 phase, defined as Ki-67$^-$. Cells were fixed for nuclear staining by using Cytofix/Cytoperm buffer according to the manufacturer's instructions (BD Biosciences).

Flow cytometry for intracellular calcium

Levels of intracellular calcium concentration in PC-3 cells were measured by flow cytometry. Fluo 3-AM, one of the most suitable $Ca2^+$ indicators, was obtained from Dojindo. Flow cytometry was performed using an Accuri C6 flow cytometer (BD Biosciences) and analyzed by FlowJo 7.6 software (TreeStar Inc.). In brief, PC-3 cells were grown on 3.5-cm dishes in medium containing 10% FBS in the presence of Wnt5a or control. The cells were washed with HBSS three times. Cells were loaded with 1 ml HBSS containing 5 µmol/liter Fluo 3-AM and incubated at 37°C for 30 min. The cells were then washed with HBSS and incubated with HBSS for 10 min. The cells were collected by centrifugation at 1,000 *g* for 5 min and resuspended in the PBS. Intracellular calcium concentration in a population of 5×10^4 cells was evaluated using a flow cytometer. The excitation wavelength was 488 nm, and emission spectra peaked at 525 nm. Fluo 3-AM is a nonratiometric fluorescent indicator. The measurement of fluorescence intensity of Fluo 3-AM is thought to approximately estimate the intracellular calcium concentration (Rijkers et al., 1990).

Cell labeling with DiD dye

Cells were stained with DiD dye (V22887; Molecular Probes), according to the manufacturer's instructions. In brief, cells (1×10^6 cells/ml) were incubated with DiD dye (0.5 µM) in serum-free media at 37°C for 40 min, washed with serum-free medium three times, and resuspended in PBS.

Immunofluorescence

5×10^3 DiD-labeled cells were plated on sterile glass coverslips, and Wnt5a was added and incubated for 1, 3, and 6 d, respectively. Then, the cells were fixed with 4% paraformaldehyde, followed by permeabilization with 0.2% Triton X-100 for 10 min at room temperature. The slips were blocked with 3% BSA for 1 h at room temperature and then incubated with primary antibodies against Ki-67 (1:200; ab66155; Abcam) at room temperature for 2 h. After washing the slips with PBS, secondary antibody FITC was incubated in the dark for 1 h at room temperature and then washed with PBS; the coverslips were counterstained with DAPI (0.1 mg/ml; Molecular Probes) and imaged with a Zeiss LSM 710 confocal microscope.

Animal study

The ethics approval statements of animal work were provided by the Institutional Animal Care and Use Committee of Sun Yat-sen University Cancer Center, and the ethics approval number for animal work was L1020120161110D. For the intracardiac model of bone metastasis, PC-3 cells (10^5 cells resuspended in 100 µl PBS) were injected into the left cardiac ventricle of BALB/c-nu mice (5–6 wk old; 18–20 g) with a 300-µl, 28.5-G insulin syringe. Successful injection was characterized by the pumping of arterial blood into the syringe. For intratibial injection model, PC-3 cells were resuspended in 100 µl PBS at the density of 2.5×10^6 cells, and 10 µl of cell solution was slowly injected with a 28.5-G needle into the tibia using a drilling motion. Mice were monitored every 3 d for bone metastases by BLI. Osteolytic lesions were identified on radiographs as radiolucent lesions in the bone. Each bone metastasis was scored as follows: 0, no metastasis; 1, bone lesion covering <1/4 of the bone width; 2, bone lesion involving 1/4–1/2 of the bone width; 3, bone lesion across 1/2–3/4 of the bone width; and 4, bone lesion >3/4 of the bone width. The bone metastasis score for each mouse was the sum of scores of all bone lesions from two hind limbs. Mice were sacrificed dependent on survival time. Two hind limbs were dissected and fixed with 4% paraformaldehyde and then decalcified by gentle shaking in decalcification solution (0.1 M Tris-HCl and 0.26 M EDTA, pH 7.4) for 3 wk and finally paraffin embedded. Then, the embedded limbs were used for H&E staining. The area of the osteolytic lesions was measured using the image analysis system MetamorphAnalysis Software (Universal Imaging Corporation), and the total extent of bone destruction per animal is expressed in square millimeters.

In the chemotherapy experiment, mice were dosed with two intraperitoneal injections of docetaxel (10 mg/kg body weight) or 0.9% NaCl solution once weekly for 2 wk (114977-28-5; LC Laboratories). In brief, the mice were randomized into the following two treatment groups: (1) consecutive treatment of Wnt5a for 56 d and then removal of Wnt5a on day 57 and (2) consecutive treatment of Wnt5a for 42 d, treatment with Wnt5a and docetaxel for 14 d, and then removal of docetaxel and Wnt5a together on day 57. The mice were culled, and the tibiae were collected and processed for confocal microscopy after 4–6 wk of docetaxel and Wnt5a removal dependent on survival time of mice.

Detection of dormant cells in vivo

Double DiD-labeled and luciferase-expressing PC-3 cells were injected into the left cardiac ventricle of the mice as described above. Mice were sacrificed on day 2 and 80 after injection, respectively, to detect the presence of double luciferase$^+$ and DiD$^+$ tumor cells in both tibiae of each mouse. Dissected tibiae were fixed with 4% paraformaldehyde and embedded in optimal cutting temperature (OCT) embedding compound (Sakura Finetek), and then frozen at −30°C before use. Serial 10 tissue sections (thickness: 10–12 µm) of both tibiae of all mice were longitudinally generated from a sagittal section with a Leica Cryostat CM3050 S. The tissue sections were stained with a rabbit anti-luciferase polyclonal antibody (L0159; Sigma) as described above. The whole fields of each slide were analyzed to detect double luciferase$^+$ and DiD$^+$ cells. Tissues were imaged on a Zeiss LSM 710 confocal microscope using either a 1.1 numerical aperture 40× water-immersion objective or a 1.4 numerical aperture 63× oil-immersion objective. The total number of double luciferase$^+$ and DiD$^+$ cells in each mouse was scored given by the two independent investigators and were statistically analyzed for further comparative number of luciferase$^+$ and DiD$^+$ cells in the indicated mice groups.

IHC

IHC analysis was performed to study altered protein expression in human PCa tissues and bone tissues. Paraffin-embedded spec-

imens were serially cut into 4-µm sections and baked at 65°C for 30 min. The sections were deparaffinized with xylenes and rehydrated. Sections were submerged into EDTA antigenic retrieval buffer and microwaved for antigenic retrieval. The sections were treated with 3% hydrogen peroxide in methanol to quench the endogenous peroxidase activity, followed by incubation with 1% BSA to block nonspecific binding. Mouse anti-Wnt5a monoclonal antibody (1:800; orb69148; Biorbyt), mouse anti-ROR2 monoclonal antibody (1:100; SAB1412202; Sigma), mouse anti-SIAH2 monoclonal antibody (1:100; S7945; Sigma) and rabbit anti–β-catenin monoclonal antibody (1:200; 9582; Cell Signaling Technology) were incubated with the sections overnight at 4°C. After washing, the tissue sections were treated with biotinylated anti-rabbit or anti-mouse secondary antibody (Zymed), followed by further incubation with streptavidin–horseradish peroxidase complex (Zymed). Staining of tissue sections was performed using 3,3′-diaminobenzidine. Sections were counterstained with hematoxylin followed by dehydration and mounting. The degree of immunostaining of formalin-fixed, paraffin-embedded sections was reviewed and scored independently by two independent investigators, based on both the proportion of positively stained tumor cells and the intensity of staining. The proportion of tumor cells was scored as follows: 0 (no positive tumor cells), 1 (<10% positive tumor cells), 2 (10–35% positive tumor cells), 3 (35–70% positive tumor cells), and 4 (>70% positive tumor cells). The staining intensity was graded according to the following criteria: 0 (no staining), 1 (weak staining, light yellow), 2 (moderate staining, yellow brown), and 3 (strong staining, brown). The staining index (SI) was calculated as staining intensity score × proportion of positive tumor cells. Using this method of assessment, we evaluated the expression of Wnt5a, ROR2, SIAH2, and nuclear β-catenin in tissues by determining SI, with scores of 0, 1, 2, 3, 4, 6, 8, 9, or 12. The median SI of each protein in all PCa tissues was used as the cutoff value to stratify high and low expression of each protein. 10 representative staining fields of each section were analyzed to procure the SI score.

Agents, primers, and plasmids

Agents

Human recombinant Wnt5a (645-WN), 5b (7347-WN), 11 (6179-WN), and 16 (7790-WN) were purchased from R&D. After 24 h of transfection, LiCl (213233; Sigma) was used to inhibit GSK-3β at 40 mM, CsA (C5207; Sigma) was used to inhibit calcineurin at 1 µM, and KN 93 (K1385; Sigma) was used to inhibit CaMKII at 25 µM. Epoxomicin (ab144598; Abcam) was used to block proteasome-mediated protein degradation at 100 nM.

Plasmids

The reporter plasmids containing wild-type (5′-CCTTTGATC-3′; TOPflash) or mutated (5′-CCTTTGGCC-3′; FOPflash) TCF/LEF DNA binding sites were purchased from Upstate Biotechnology. The shRNA for *Wnt5a* and *ROR2*, the mutant form of β-catenin lacking amino acids 29–48, Δβ-catenin, the dominant negative *SIAH1* (ΔSIAH1), *SIAH2* (ΔSIAH2), and *Ebi* (ΔEbi) were synthesized by Vigene Biosciences, and the sequences are listed below.

Wnt5a, RNAi no. 1: 5′-CCGGCTAGTGGCTTTGGCCATATTTCT CGAGAAATATGGCCAAAGCCACTAGTTTTTG-3′; RNAi no. 2: 5′-CCGGCTCCCAGGACCCGCTTATTTACTCGAGTAAATAAGCGGGTC CTGGGAGTTTTTG-3′.

ROR2, RNAi no. 1: 5′-CCGGCCTCATTAACCAGCACAAACACT CGAGTGTTTGTGCTGGTTAATGAGGTTTTTG-3′; RNAi no. 2: CCGGGCACAGCCCAAATCATAACTTCTCGAGAAGTTATGATTTGG GCTGTGCTTTTTG.

Δβ-catenin, 5′-ATGGCTACTCAAGCTGATTTGATGGAGTTG GACATGGCCATGGAACCAGACAGAAAAGCGGCTGTTAGTCAC TGGCAGCAACAGAAAGGCAATCCTGAGGAAGAGGATGTGGAT ACCTCCCAAGTCCTGTATGAGTGGGAACAGGGATTTTCTCAG TCCTTCACTCAAGAACAAGTAGCTGATATTGATGGACAGTAT GCAATGACTCGAGCTCAGAGGGTACGAGCTGCTATGTTCCC TGA GACATTAGATGAGGGCATGCAGATCCCATCTACACAGTTTGATGC TGCTCATCCCACTAATGTCCAGCGTTTGGCTGAACCATCACAGAT GCTGAAACATGCAGTTGTAAACTTGATTAACTATCAAGATGATGC AGAACTTGCCACACGTGCAATCCCTGAACTG ACAAAACTGCTA AATGACGAGGACCAGGTGGTGGTTAATAAGGCTGCAGTTATG GTCCATCAGCTTTCTAAAAAGGAAGCTTCCAGACACGCTATC ATGCGTTCTCCTCAGATGGTGTCTGCTATTGTACGTACCATGCAG AATACAAATGAT GTAGAAACAGCTCGTTGTACCGCTGGGACC TTGCATAACCTTTCCCATCATCGTGAGGGCTTACTGGCCATCTTT AAGTCTGGAGGCATTCCTGCCCTGGTGAAAATGCTTGGTTCA CCAGTGGATTCTGTGTTGTTTTATGCCATTACAACTCTCCACAAC CTTT TATTACATCAAGAAGGAGCTAAAATGGCAGTGCGTTTAG CTGGTGGGCTGCAGAAAATGGTTGCCTTGCTCAACAAAACAA ATGTTAAATTCTTGGCTATTACGACAGACTGCCTTCAAATTTTAG CTTATGGCAACCAAGAAAGCAAGCTCATCATACTGGCTAGTGGTG GACCCCAAGCTTTAGTAAATATAATGAGGACCTATACTTACGAAA AACTACTGTGGACCACAAGCAGAGTGCTGAAGGTGCTATCTGTCT GCTCTAGTAATAAGCCGGCTATTGTAGAA GCTGGTGGAATGCAA GCTTTAGGACTTCACCTGACAGATCCAAGTCAACGTCTTGTTCAG AACTGTCTTTGGACTCTCAGGAATCTTTCAGATGCTGCAACTAAA CAGGAAGGGATGGAAGGTCTCCTTGGGACTCTTGTTCAGCTT CTGGGTTCAGATGATATAAATGTGGTCACCTGTGCAGCTGGA ATTCTTTCTAACCTCAC TTGCAATAATTATAAGAACAAGATGAT GGTCTGCCAAGTGGGTGGTATAGAGGCTCTTGTGCGTACTGT CCTTCGGGCTGGTGACAGGGAAGACATCACTGAGCCTGCCAT CTGTGCTCTTCGTCATCTGACCAGCCGACACCAAGAAGCAGA GATGGCCCAGAATGCAGTTCGCCTTCACTATGGACT ACCAGT TGTGGTTAAGCTCTTACACCCACCATCCCACTGGCCTCTGATAAA GGCTACTGTTGGATTGATTCGAAATCTTGCCCTTTGTCCCGCAAA TCATGCACCTTTGCGTGAGCAGGGTGCCATTCCACGACTAGTTCA GTTGCTTGTTCGTGCACATCAGGATACCCAGCG CCGTACGTCCAT GGGTGGGACACAGCAGCAATTTGTGGAGGGGGTCCGCATGGA AGAAATAGTTGAAGGTTGTACCGGAGCCCTTCACATCCTAGC TCGGGATGTTCACAACCGAATTGTTATCAGAGGACTAAATAC CATTCCATTGTTTGTGCAGCTGCTTTATTCTCCCATTGAAAACAT CCA AAGAGTAGCTGCAGGGGTCCTCTGTGAACTTGCTCAGGA CAAGGAAGCTGCAGAAGCTATTGAAGCTGAGGGAGCCACAGC TCCTCTGACAGAGTTACTTCACTCTAGGAATGAAGGTGTGGCGAC ATATGCAGCTGCTGTTTTGTTCCGAATGTCTGAGGACAAGCCACA AGATTACAAGAAACGGCTTTCAGTTGAGCTGACCAGCTCTCTCTT CAGAACAGAGCCAATGGCTTGGAATGAGACTGCTGATCTTGG ACTTGATATTGGTGCCCAGGGAGAACCCCTTGGATATCGCCAGGA TGATCCTAGCTATCGTTCTTTTCACTCTGGTGGATATGGCCAGGA TGCCTTGGGTATGGACCCCAT GATGGAACATGAGATGGGTGG CCACCACCCTGGTGCTGACTATCCAGTTGATGGGCTGCCAGATCT

GGGGCATGCCCAGGACCTCATGGATGGGCTGCCTCCAGGTGA CAGCAATCAGCTGGCCTGGTTTGATACTGACCTG-3′.

ΔSIAH1: 5′-ATGGTGGCTAATTCAGTACTTTTCCCCTGTAAA TATGCGTCTTCTGGATGTGAAATAACTCTGCCACACACAGAA AAAGCAGACCATGAAGAGCTCTGTGAGTTTAGGCCTTATTCC TGTCCGTGCCCTGGTGCTTCCT GTAAATGGCAAGGCTCTCTGG ATGCTGTAATGCCCCATCTGATGCATCAGCATAAGTCCATTACAA CCCTACAGGGAGAGGATATAGTTTTTCTTGCTACAGACATTAAT CTTCCTGGTGCTGTTGACTGGGTGATGATGCAGTCCTGTTTT GGCTTTCACTTCATGTTAGTCTTAGAGAAACAGGAAAAATAC GATGGTCACCAGCAGTTCTTCGCAATCGTACAGCTGATAGGAACA CGCAAGCAAGCTGAAAATTTTGCTTACCGACTTGAGCTAAA TGG TCATAGGCGACGATTGACTTGGGAAGCGACTCCTCGATCTATTCA TGAAGGAATTGCAACAGCCATTATGAATAGCGACTGTCTAGTCTT TGACACCAGCATTGCACAGCTTTTTGCAGAAAATGGCAATTT AGGCATCAATGTAACTATTTCCATGTGT-3′.

ΔSIAH2: 5′-ATGGTGGCCTCGGCAGTCCTGTTTCCCTGTAAG TATGCCACCACGGGCTGTTCCCTGACCCTGCACCATACGGAGAAA CCAGAACATGAAGACATATGTGAATACCGTCCCTACTCCTGCCCA TGTCCTGGTGCTTCCT GCAAGTGGCAGGGGTCCCTGGAAGCTG TGATGTCCCATCTCATGCACGCCCACAAGAGCATTACCACCCTTC AGGGAGAAGACATCGTCTTTCTAGCTACAGACATTAAC TTGCCA GGGGCTGTCGACTGGGTGATGATGCAGTCATGTTTTGGCCAT CACTTCATGCTGGTGCTGGAGAAACAAGAGAAGTACGAAGGC CACCAGCAGTTTTTTGCCATCGTCCTGCTCATTGGCACCCGCAAG CAAGCCGAGAACTTTGCCTACAGACTGGAGTTGAA TGGGAACCG GCGGAGATTGACCTGGGAGGCCACGCCCCGTTCGATTCATGA CGGTGTGGCTGCGGCCATCATGAACAGCGACTGCCTTGTTTT CGACACAGCCATAGCACATCTTTTTGCAGATAATGGGAACCTTGG AATCAATGTTACTATTTCTACATGT-3′.

Ebi(ΔF): 5′-ATGACCGAGCTCGCTGGCGCCTCTTCATCGTGC TGCCACCGCCCTGCAGGAAGAGGGGCCATGCAGTCAGTCTTG CACCACTTTCAACGTTTGCGAGGGAGAGAGGGTGGTTCCCAC TTCATCAACACCTCATCGC CGCGAGGTGAGGCTAAGATGAGCA TAACCAGTGACGAGGTGAACTTTCTGGTGTATCGGTATCTCC AGGAGTCAGGTTTTTCCCACTCGGCTTTCACGTTTGGGATTG AGA GCCACATCAGCCAGTCCAACATCAATGTGATGCCCGACG TGGTGCAGACGCGGCAGCAGGCATTCCGAGAGAAGCTCGCTC AGCAGCAAGCCAGTGCGGCGGCGGCGGCGGCTGCGGCCACGG CAGCAGCGACAGCAGCCACCACGACCTCAGCCGGCGTTTCCC ACCA AAATCCATCGAAGAACAGAGAGGCCACGGTGAATGGGGA AGAGAACAGAGCACATTCAGTCAATAATCACGCGAAGCCAAT GGAAATAGATGGAGAGGTTGAGATTCCATCCAGCAAAGCCAC AGTCCTTCGGGGCCATGAGTCTGAGGTGT TCATTTGTGCCTGGA ATCCTGTCAGTGATTTGCTAGCCTCCGGATCTGGAGACTCAACTG CAAGGATATGGAACCTGAATGAGAATAGCAACGGGGGCTCCA CCCAGCTCGTGTTGAGGCACTGTATACGAGAGGGGGGCCATG ACGTCCCGAGTAACAAAGACGT CACCTCACTGGACTGGAATAC CAATGGAACACTCTTGGCTACGGGTTCATATGACGGTTTTGC AAGAATATGGACGGAAGATGGTAACCTGGCCAGCACCTTAGG CCAACATAAAGGCCCCATCTTTGCCTTGAAATGGAACCGAAA GGGGAATTACATTTTGAGTGCTGGTGTAGACAAAACAACAAT AATTTGGGATGCCCACACAGGAGAAGCCAAACAGCAGTTTCC TTTTCATTCAGCCCCTGCCCTTGATGTGGACTGGCAGAACAA CACGACCTTTGCCT CCTGTAGCACAGACATGTGTATCCATGTGT GCAGGCTCGGCTGTGACCGCCCAGTCAAAACCTTCCAGGGAC ACACAAACGAGGTCAACGCCATCAAATGGGATCCGTCTGGAA TGTTGCTGGCATCCTGCTCGGATGACATGACATTGAAGATCTGGA GCATGAAACAGGAGGTGTGCATCCATGATCTTCAGGCTCACAATA AAGAGATCTA CACCATCAAGTGGAGCCCCACTGGGCCCGCCAC CAGCAACCCAAACTCCAACATCATGTTGGCAAGTGCTTCGTT TGATTCTACGGTGCGACTGTGGGACATAGAACGAGGCGTCTG CACCCACACGCTCACGAAGCATCAGGAGCCTGTCTATAGCGTAGC TTTCAGCCCTGATGGGAAGTACTT GGCCAGTGGATCCTTCGA CAAGTGCGTCCATATCTGGAATACTCAGAGTGGAAATCTTGTCCA CAGCTACCGAGGCACTGGCGGCATCTTCGAGGTGTGCTGGAA CGCCCGAGGAGACAAAGTGGGTGCCAGCGCGTCCGACGGC TCT GTGTGTGTTTTGGATCTGCGGAAG-3′.

"Δ" means mutational; "ΔF" means the sequence of F-box in Ebi had been cut off.

Primers

CCND1 forward, 5′-GCCCTCGGTGTCCTACTTC-3′; *CCND1* reverse, 5′-CTCCTCCTCGCACTTCTGTT-3′; *CCND2* forward, 5′-GGT CGGGTTTTCAATCACAC-3′; *CCND2* reverse, 5′-CCTCTTCACCTC CCTTCAACT-3′; *CCND3* forward, 5′-TCCTCTCCCATTGTCCCTCT-3′; *CCND3* reverse, 5′-CCACCAGCCTAAACCTTGC-3′; *CCNA1* forward, 5′-GGAAGGCATTTTCTGATCCA-3′; *CCNA1* reverse, 5′-GCT AGGGCTGCTAACTGCAA-3′; *CCNA2* forward, 5′-ATGTCACCGTTC CTCCTTG-3′; *CCNA2* reverse, 5′-GGGCATCTTCACGCTCTATT-3′; *CCNB1* forward, 5′-TGAGGAAGAGCAAGCAGTCA-3′; *CCNB1* reverse, 5′-ATGGTCTCCTGCAACAACCT-3′; *CCNB2* forward, 5′-ACT GCTCTGCTCTTGGCTTC-3′; *CCNB2* reverse, 5′-TTTCTCGGATTT GGGAACTG-3′; *CCNB3* forward, 5′-AGATCCACCAGCTTCACTGC-3′; *CCNB3* reverse, 5′-GTGACATGAGGGCCATTCTT-3′; *CCNE1* forward, 5′-CGGTATATGGCGACACAAGA-3′; *CCNE1* reverse, 5′-ACA TACGCAAACTGGTGCAA-3′; *CCNE2* forward, 5′-AGGAAAACT ACCCAGGATGTCA-3′; *CCNE2* reverse, 5′-ATCAGGCAAAGGTGA AGGATTA-3′; *CDK1* forward, 5′-GGTCAAGTGGTAGCCATGAAA-3′; *CDK1* reverse, 5′-CCAGGAGGGATAGAATCCAAG-3′; *CDK2* forward, 5′-TGCCTGATTACAAGCCAAGTT-3′; *CDK2* reverse, 5′-GAG TCGAAGATGGGGTACTGG-3′; *CDK4* forward, 5′-CAGCTACCA GATGGCACTTACA-3′; *CDK4* reverse, 5′-CAAAGATACAGCCAA CACTCCA-3′; *CDK6* forward, 5′-GTCAGGTTGTTTGATGTGTGC-3′; *CDK6* reverse, 5′-CGGTGTGAATGAAGAAAGTCC-3′; *CDKN1A* forward, 5′-AGGTGGACCTGGAGACTCTCAG-3′; *CDKN1A* reverse, 5′-TCCTCTTGGAGAAGATCAGCCG-3′; *CDKN1B* forward, 5′-ATA AGGAAGCGACCTGCAACCG-3′; *CDKN1B* reverse, 5′-TTCTTGGGC GTCTGCTCCACAG-3′; *RB1* forward, 5′-CAGAAGGTCTGCCAACAC CAAC-3′; *RB1* reverse, 5′-TTGAGCACACGGTCGCTGTTAC-3′; *Wnt1* forward, 5′-ATAGCCTCCTCCACGAACCT-3′; *Wnt1* reverse, 5′-GGA ATTGCCATTTGCACTCT-3′; *Wnt2* forward, 5′-GGTCAGCTCTTC ATGGTGGT-3′; *Wnt2* reverse, 5′-ATCTCTGTCCAGGGTGTTGC-3′; *Wnt2b* forward, 5′-TCAACGCTACCCAGACATCA-3′; *Wnt2b* reverse, 5′-ACCACTCCTGCTGACGAGAT-3′; *Wnt3* forward, 5′-AGG AGTGCCAGCATCAGTTC-3′; *Wnt3* reverse, 5′-ACTTCCAGCCTT CTCCAGGT-3′; *Wnt3a* forward, 5′-CTGGCAGCTGTGAAGTGAAG-3′; *Wnt3a* reverse, 5′-TGGGTGAGGCCTCGTAGTAG-3′; *Wnt4* forward, 5′-CTGGAGAAGTGTGGCTGTGA-3′; *Wnt4* reverse, 5′-CAG CCTCGTTGTTGTGAAGA-3′; *Wnt5a* forward, 5′-CAAATAGGCAGC CGAGAGAC-3′; *Wnt5a* reverse, 5′-CTCTAGCGTCCACGAACTCC-3′; *Wnt5b* forward, 5′-CTGCTTGCGTAATGAGACCA-3′; *Wnt5b* reverse, 5′-AAAGCAACACCAGTGGAACC-3′; *Wnt6* forward, 5′-TCA GTTCCAGTTCCGTTTCC-3′; *Wnt6* reverse, 5′-CATGGAACAGGC

TTGAGTGA-3′; *Wnt7a* forward, 5′-GGTGCGAGCATCATCTGTAA-3′; *Wnt7a* reverse, 5′-TCCTTCCCGAAGACAGTACG-3′; *Wnt7b* forward, 5′-AAGCCTATGGAGACGGACCT-3′; *Wnt7b* reverse, 5′-TTG GTGTACTGGTGCGTGTT-3′; *Wnt8a* forward, 5′-AGCACAGAGGCT GAGCTGAT-3′; *Wnt8a* reverse, 5′-TCTGCTCTCCTCTCCTCCAC-3′; *Wnt8b* forward, 5′-GTGGACTTCGAAGCGCTAAC-3′; *Wnt8b* reverse, 5′-CTGCTTGGAAATTGCCTCTC-3′; *Wnt9a* forward, 5′-TGCTTTCCTCTACGCCATCT-3′; *Wnt9a* reverse, 5′-CCTTGACAA ACTTGCTGCTG-3′; *Wnt9b* forward, 5′-TGGAGCGCTGTACTTGTG AC-3′; *Wnt9b* reverse, 5′-GCACTTGCAGGTTGTTCTCA-3′; *Wnt10a* forward, 5′-CATGAGTGCCAGCATCAGTT-3′; *Wnt10a* reverse, 5′-ACCGCAAGCCTTCAGTTTAC-3′; *Wnt10b* forward, 5′-GGAAGG GTAGTGGTGAGCAA-3′; *Wnt10b* reverse, 5′-CTCTCCGAAGTC CATGTCGT-3′; *Wnt11* forward, 5′-CAGGATCCCAAGCCAATA AA-3′; *Wnt11* reverse, 5′-GTAGCGGGTCTTGAGGTCAG-3′; *Wnt16* forward, 5′-GAGCTGTGCAAGAGGAAACC 3′; *Wnt16* reverse, 5′-TGAATGCTGTCTCCTTGGTG-3′; *MYC* forward, 5′-CCTGGTGCT CCATGAGGAGAC-3′; *MYC* reverse, 5′-CAGACTCTGACCTTTTGC CAGG-3′; *CD44* forward, 5′-CCAGAAGGAACAGTGGTTTGGC-3′; *CD44* reverse, 5′-ACTGTCCTCTGGGCTTGGTGTT-3′; *JUN* forward, 5′-CCTTGAAAGCTCAGAACTCGGAG-3′; *JUN* reverse, 5′-TGCTGCGTTAGCATGAGTTGGC-3′; *LEF1* forward, 5′-CTACCC ATCCTCACTGTCAGTC-3′; *LEF1* reverse, 5′-GGATGTTCCTGTTTG ACCTGAGG-3′; *HNF1A* forward, 5′-AGACGCTAGTGGAGGAGT GCAA-3′; *HNF1A* reverse, 5′-GGCAAACCAGTTGTAGACACGC-3′; *AXIN2* forward, 5′-CAAACTTTCGCCAACCGTGGTTG-3′; *AXIN2* reverse, 5′-GGTGCAAAGACATAGCCAGAACC-3′; *VEFGA* forward, 5′-TTGCCTTGCTGCTCTACCTCCA-3′; *VEFGA* reverse, 5′-GATGGC AGTAGCTGCGCTGATA-3′; *MMP7* forward, 5′-TCGGAGGAGATG CTCACTTCGA-3′; *MMP7* reverse, 5′-GGATCAGAGGAATGTCCC ATACC-3′; *SIAH1* forward, 5′-TCTTCCTGGTGCTGTTGACTGG-3′; *SIAH1* reverse, 5′-CGATTGCGAAGAACTGCTGGTG-3′; *SIAH2* forward, 5′-GCATCAGGAACCTGGCTATGGA-3′; *SIAH2* reverse, 5′-GCAGGAGTAGGGACGGTATTCA-3′; *ROR2* forward, 5′-GTA CGCATGGAACTGTGTGACG-3′; *ROR2* reverse, 5′-AAAGGCAAG CGATGACCAGTGG-3′; *GAPDH* forward, 5′-ATTCCACCCATGGCA AATTC-3′; *GAPDH* reverse, 5′-TGGGATTTCCATTGATGACAAG-3′.

Statistical analysis

All values are presented as means ± SD. Significant differences were evaluated using GraphPad 5.0 software. Student's *t* test was used to determine significant differences between two groups. The χ^2 test was used to analyze the relationship between ROR2 expression and clinicopathological characteristics in PCa patients. A two-tailed P value of <0.05 was considered statistically significant in all experiments. All experiments were repeated three times.

Online supplemental material

Fig. S1 shows the isolation and stainings of primary osteoblasts from the calvaria of neonatal rats. Fig. S2 shows that Wnt5a from different cell components of the osteoblastic niche inhibits proliferation of PCa cells. Fig. S3 demonstrates that Wnt5a antagonizes canonical Wnt/β-catenin signaling independent of Wnt/Ca^{2+} signaling and GSK-3β. Fig. S4 demonstrates that ROR2/SIAH2 signaling mediates the roles of Wnt5a in inducing the dormancy of PCa cells in bone. Fig. S5 shows the isolation and establishment of primary PCa cells from clinical PCa tissues. Table S1 shows the clinicopathological characteristics of 231 PCa patients whose samples were used for IHC analysis.

Acknowledgments

We would like to thank Junchao Cai from the Department of Microbiology at the Sun Yat-sen University for his advice and insights and Yubo Tang from the Department of Pharmacy at The First Affiliated Hospital of Sun Yat-sen University for irradiated Swiss 3T3 J2 mouse fibroblasts.

This work was supported by grants from the National Natural Science Foundation of China (nos. 81472505 and 81530082) and The Ministry of Science and Technology of China grant (973 Program, no. 2014CB910604).

The authors declare no competing financial interests.

Author contributions: L. Song and X. Peng developed ideas and drafted the manuscript. D. Ren, Y. Dai, and Q. Yang conducted the experiments and contributed to the analysis of data. X. Zhang, W. Guo, L. Ye, Y. Lai, and H. Du contributed to the analysis of data. S. Huang and X. Chen conducted the experiments. C. Lin edited the manuscript. All authors contributed to revise the manuscript and approved the final version for publication.

Submitted: 9 April 2018
Revised: 31 October 2018
Accepted: 28 November 2018

References

Aguirre-Ghiso, J.A. 2007. Models, mechanisms and clinical evidence for cancer dormancy. *Nat. Rev. Cancer.* 7:834–846. https://doi.org/10.1038/nrc2256

Amin, R., Y. Morita-Fujimura, H. Tawarayama, K. Semba, N. Chiba, M. Fukumoto, and S. Ikawa. 2016. ΔNp63α induces quiescence and downregulates the BRCA1 pathway in estrogen receptor-positive luminal breast cancer cell line MCF7 but not in other breast cancer cell lines. *Mol. Oncol.* 10:575–593. https://doi.org/10.1016/j.molonc.2015.11.009

Andersen, T.L., T.E. Sondergaard, K.E. Skorzynska, F. Dagnaes-Hansen, T.L. Plesner, E.M. Hauge, T. Plesner, and J.M. Delaisse. 2009. A physical mechanism for coupling bone resorption and formation in adult human bone. *Am. J. Pathol.* 174:239–247. https://doi.org/10.2353/ajpath.2009.080627

Banerjee, S., M. Hussain, Z. Wang, A. Saliganan, M. Che, D. Bonfil, M. Cher, and F.H. Sarkar. 2007. In vitro and in vivo molecular evidence for better therapeutic efficacy of ABT-627 and taxotere combination in prostate cancer. *Cancer Res.* 67:3818–3826. https://doi.org/10.1158/0008-5472.CAN-06-3879

Bowers, M., B. Zhang, Y. Ho, P. Agarwal, C.C. Chen, and R. Bhatia. 2015. Osteoblast ablation reduces normal long-term hematopoietic stem cell self-renewal but accelerates leukemia development. *Blood.* 125:2678–2688. https://doi.org/10.1182/blood-2014-06-582924

Buczacki, S.J.A., S. Popova, E. Biggs, C. Koukorava, J. Buzzelli, L. Vermeulen, L. Hazelwood, H. Francies, M.J. Garnett, and D.J. Winton. 2018. Itraconazole targets cell cycle heterogeneity in colorectal cancer. *J. Exp. Med.* 215:1891–1912.

Cai, J., H. Guan, L. Fang, Y. Yang, X. Zhu, J. Yuan, J. Wu, and M. Li. 2013. MicroRNA-374a activates Wnt/β-catenin signaling to promote breast cancer metastasis. *J. Clin. Invest.* 123:566–579.

Canesin, G., S. Evans-Axelsson, R. Hellsten, A. Krzyzanowska, C.P. Prasad, A. Bjartell, and T. Andersson. 2017. Treatment with the WNT5A-mimicking peptide Foxy-5 effectively reduces the metastatic spread of WNT5A-low prostate cancer cells in an orthotopic mouse model. *PLoS One.* 12:e0184418. https://doi.org/10.1371/journal.pone.0184418

Croucher, P.I., M.M. McDonald, and T.J. Martin. 2016. Bone metastasis: the importance of the neighbourhood. *Nat. Rev. Cancer.* 16:373–386. https://doi.org/10.1038/nrc.2016.44

D'Souza, S., N. Kurihara, Y. Shiozawa, J. Joseph, R. Taichman, D.L. Galson, and G.D. Roodman. 2012. Annexin II interactions with the annexin II receptor enhance multiple myeloma cell adhesion and growth in the bone marrow microenvironment. *Blood.* 119:1888–1896. https://doi.org/10.1182/blood-2011-11-393348

Da Forno, P.D., J.H. Pringle, P. Hutchinson, J. Osborn, Q. Huang, L. Potter, R.A. Hancox, A. Fletcher, and G.S. Saldanha. 2008. WNT5A expression increases during melanoma progression and correlates with outcome. *Clin. Cancer Res.* 14:5825–5832. https://doi.org/10.1158/1078-0432.CCR-07-5104

Dey-Guha, I., A. Wolfer, and A.C. Yeh. G.A. J, R. Darp, E. Leon, J. Wulfkuhle, E.F. Petricoin, 3rd, B.S. Wittner, and S. Ramaswamy. 2011. Asymmetric cancer cell division regulated by AKT. *Proceedings of the National Academy of Sciences of the United States of America* 108:12845-12850.

Døsen, G., E. Tenstad, M.K. Nygren, H. Stubberud, S. Funderud, and E. Rian. 2006. Wnt expression and canonical Wnt signaling in human bone marrow B lymphopoiesis. *BMC Immunol.* 7:13. https://doi.org/10.1186/1471-2172-7-13

Ebinger, S., E.Z. Özdemir, C. Ziegenhain, S. Tiedt, C. Castro Alves, M. Grunert, M. Dworzak, C. Lutz, V.A. Turati, T. Enver, et al. 2016. Characterization of Rare, Dormant, and Therapy-Resistant Cells in Acute Lymphoblastic Leukemia. *Cancer Cell.* 30:849–862. https://doi.org/10.1016/j.ccell.2016.11.002

Ell, B., and Y. Kang. 2012. SnapShot: Bone Metastasis. *Cell.* 151:690–690.e1. https://doi.org/10.1016/j.cell.2012.10.005

Esposito, M., T. Guise, and Y. Kang. 2018. The Biology of Bone Metastasis. *Cold Spring Harb. Perspect. Med.* 8:a031252. https://doi.org/10.1101/cshperspect.a031252

Essers, M.A., and A. Trumpp. 2010. Targeting leukemic stem cells by breaking their dormancy. *Mol. Oncol.* 4:443–450. https://doi.org/10.1016/j.molonc.2010.06.001

Fidler, I.J. 1970. Metastasis: quantitative analysis of distribution and fate of tumor emboli labeled with 125 I-5-iodo-2′-deoxyuridine. *J. Natl. Cancer Inst.* 45:773–782.

Ishitani, T., S. Kishida, J. Hyodo-Miura, N. Ueno, J. Yasuda, M. Waterman, H. Shibuya, R.T. Moon, J. Ninomiya-Tsuji, and K. Matsumoto. 2003. The TAK1-NLK mitogen-activated protein kinase cascade functions in the Wnt-5a/Ca(2+) pathway to antagonize Wnt/beta-catenin signaling. *Mol. Cell. Biol.* 23:131–139. https://doi.org/10.1128/MCB.23.1.131-139.2003

Jönsson, M., J. Dejmek, P.O. Bendahl, and T. Andersson. 2002. Loss of Wnt-5a protein is associated with early relapse in invasive ductal breast carcinomas. *Cancer Res.* 62:409–416.

Jung, Y., A.M. Decker, J. Wang, E. Lee, L.A. Kana, K. Yumoto, F.C. Cackowski, J. Rhee, P. Carmeliet, L. Buttitta, et al. 2016. Endogenous GAS6 and Mer receptor signaling regulate prostate cancer stem cells in bone marrow. *Oncotarget.* 7:25698–25711. https://doi.org/10.18632/oncotarget.8365

Karadag, A., B.O. Oyajobi, J.F. Apperley, R.G. Russell, and P.I. Croucher. 2000. Human myeloma cells promote the production of interleukin 6 by primary human osteoblasts. *Br. J. Haematol.* 108:383–390. https://doi.org/10.1046/j.1365-2141.2000.01845.x

Kim, S.E., J.Y. Yoon, W.J. Jeong, S.H. Jeon, Y. Park, J.B. Yoon, Y.N. Park, H. Kim, and K.Y. Choi. 2009. H-Ras is degraded by Wnt/beta-catenin signaling via beta-TrCP-mediated polyubiquitylation. *J. Cell Sci.* 122:842–848. https://doi.org/10.1242/jcs.040493

Kingsley, L.A., P.G. Fournier, J.M. Chirgwin, and T.A. Guise. 2007. Molecular biology of bone metastasis. *Mol. Cancer Ther.* 6:2609–2617. https://doi.org/10.1158/1535-7163.MCT-07-0234

Klein, P.S., and D.A. Melton. 1996. A molecular mechanism for the effect of lithium on development. *Proc. Natl. Acad. Sci. USA.* 93:8455–8459. https://doi.org/10.1073/pnas.93.16.8455

Kobayashi, A., H. Okuda, F. Xing, P.R. Pandey, M. Watabe, S. Hirota, S.K. Pai, W. Liu, K. Fukuda, C. Chambers, et al. 2011. Bone morphogenetic protein 7 in dormancy and metastasis of prostate cancer stem-like cells in bone. *J. Exp. Med.* 208:2641–2655. https://doi.org/10.1084/jem.20110840

Koebel, C.M., W. Vermi, J.B. Swann, N. Zerafa, S.J. Rodig, L.J. Old, M.J. Smyth, and R.D. Schreiber. 2007. Adaptive immunity maintains occult cancer in an equilibrium state. *Nature.* 450:903–907. https://doi.org/10.1038/nature06309

Kremenevskaja, N., R. von Wasielewski, A.S. Rao, C. Schöfl, T. Andersson, and G. Brabant. 2005. Wnt-5a has tumor suppressor activity in thyroid carcinoma. *Oncogene.* 24:2144–2154. https://doi.org/10.1038/sj.onc.1208370

Kühl, M., L.C. Sheldahl, C.C. Malbon, and R.T. Moon. 2000. Ca(2+)/calmodulin-dependent protein kinase II is stimulated by Wnt and Frizzled homologs and promotes ventral cell fates in Xenopus. *J. Biol. Chem.* 275:12701–12711. https://doi.org/10.1074/jbc.275.17.12701

Lambert, A.W., D.R. Pattabiraman, and R.A. Weinberg. 2017. Emerging Biological Principles of Metastasis. *Cell.* 168:670–691. https://doi.org/10.1016/j.cell.2016.11.037

Lawson, M.A., M.M. McDonald, N. Kovacic, W. Hua Khoo, R.L. Terry, J. Down, W. Kaplan, J. Paton-Hough, C. Fellows, J.A. Pettitt, et al. 2015. Osteoclasts control reactivation of dormant myeloma cells by remodelling the endosteal niche. *Nat. Commun.* 6:8983. https://doi.org/10.1038/ncomms9983

Liu, J., J. Stevens, C.A. Rote, H.J. Yost, Y. Hu, K.L. Neufeld, R.L. White, and N. Matsunami. 2001. Siah-1 mediates a novel beta-catenin degradation pathway linking p53 to the adenomatous polyposis coli protein. *Mol. Cell.* 7:927–936. https://doi.org/10.1016/S1097-2765(01)00241-6

Lu, Z., R.Z. Luo, Y. Lu, X. Zhang, Q. Yu, S. Khare, S. Kondo, Y. Kondo, Y. Yu, G.B. Mills, et al. 2008. The tumor suppressor gene ARHI regulates autophagy and tumor dormancy in human ovarian cancer cells. *J. Clin. Invest.* 118:3917–3929.

Luzzi, K.J., I.C. MacDonald, E.E. Schmidt, N. Kerkvliet, V.L. Morris, A.F. Chambers, and A.C. Groom. 1998. Multistep nature of metastatic inefficiency: dormancy of solitary cells after successful extravasation and limited survival of early micrometastases. *Am. J. Pathol.* 153:865–873. https://doi.org/10.1016/S0002-9440(10)65628-3

Maeda, K., Y. Kobayashi, N. Udagawa, S. Uehara, A. Ishihara, T. Mizoguchi, Y. Kikuchi, I. Takada, S. Kato, S. Kani, et al. 2012. Wnt5a-Ror2 signaling between osteoblast-lineage cells and osteoclast precursors enhances osteoclastogenesis. *Nat. Med.* 18:405–412. https://doi.org/10.1038/nm.2653

Malladi, S., D.G. Macalinao, X. Jin, L. He, H. Basnet, Y. Zou, E. de Stanchina, and J. Massagué. 2016. Metastatic Latency and Immune Evasion through Autocrine Inhibition of WNT. *Cell.* 165:45–60. https://doi.org/10.1016/j.cell.2016.02.025

Matsuzawa, S.I., and J.C. Reed. 2001. Siah-1, SIP, and Ebi collaborate in a novel pathway for beta-catenin degradation linked to p53 responses. *Mol. Cell.* 7:915–926. https://doi.org/10.1016/S1097-2765(01)00242-8

Meng, L., R. Mohan, B.H. Kwok, M. Elofsson, N. Sin, and C.M. Crews. 1999. Epoxomicin, a potent and selective proteasome inhibitor, exhibits in vivo antiinflammatory activity. *Proc. Natl. Acad. Sci. USA.* 96:10403–10408. https://doi.org/10.1073/pnas.96.18.10403

Mikels, A.J., and R. Nusse. 2006. Purified Wnt5a protein activates or inhibits beta-catenin-TCF signaling depending on receptor context. *PLoS Biol.* 4:e115. https://doi.org/10.1371/journal.pbio.0040115

Naumov, G.N., E. Bender, D. Zurakowski, S.Y. Kang, D. Sampson, E. Flynn, R.S. Watnick, O. Straume, L.A. Akslen, J. Folkman, and N. Almog. 2006. A model of human tumor dormancy: an angiogenic switch from the nonangiogenic phenotype. *J. Natl. Cancer Inst.* 98:316–325. https://doi.org/10.1093/jnci/djj068

Nemeth, M.J., L. Topol, S.M. Anderson, Y. Yang, and D.M. Bodine. 2007. Wnt5a inhibits canonical Wnt signaling in hematopoietic stem cells and enhances repopulation. *Proc. Natl. Acad. Sci. USA.* 104:15436–15441. https://doi.org/10.1073/pnas.0704747104

Nishita, M., M. Enomoto, K. Yamagata, and Y. Minami. 2010. Cell/tissue-tropic functions of Wnt5a signaling in normal and cancer cells. *Trends Cell Biol.* 20:346–354. https://doi.org/10.1016/j.tcb.2010.03.001

Orriss, I.R., S.E. Taylor, and T.R. Arnett. 2012. Rat osteoblast cultures. *Methods Mol. Biol.* 816:31–41. https://doi.org/10.1007/978-1-61779-415-5_3

Paget, S. 1989. The distribution of secondary growths in cancer of the breast. 1889. *Cancer Metastasis Rev.* 8:98–101.

Pantel, K., and R.H. Brakenhoff. 2004. Dissecting the metastatic cascade. *Nat. Rev. Cancer.* 4:448–456. https://doi.org/10.1038/nrc1370

Parish, C.L., G. Castelo-Branco, N. Rawal, J. Tonnesen, A.T. Sorensen, C. Salto, M. Kokaia, O. Lindvall, and E. Arenas. 2008. Wnt5a-treated midbrain neural stem cells improve dopamine cell replacement therapy in parkinsonian mice. *J. Clin. Invest.* 118:149–160. https://doi.org/10.1172/JCI32273

Pound, C.R., A.W. Partin, M.A. Eisenberger, D.W. Chan, J.D. Pearson, and P.C. Walsh. 1999. Natural history of progression after PSA elevation following radical prostatectomy. *JAMA.* 281:1591–1597. https://doi.org/10.1001/jama.281.17.1591

Price, T.T., M.L. Burness, A. Sivan, M.J. Warner, R. Cheng, C.H. Lee, L. Olivere, K. Comatas, J. Magnani, H. Kim Lyerly, et al. 2016. Dormant breast cancer micrometastases reside in specific bone marrow niches that regulate their transit to and from bone. *Sci. Transl. Med.* 8:340ra73. https://doi.org/10.1126/scitranslmed.aad4059

Rauner, M., W. Sipos, and P. Pietschmann. 2008. Age-dependent Wnt gene expression in bone and during the course of osteoblast differentiation. *Age (Dordr.)*. 30:273–282. https://doi.org/10.1007/s11357-008-9069-9

Rijkers, G.T., L.B. Justement, A.W. Griffioen, and J.C. Cambier. 1990. Improved method for measuring intracellular Ca++ with fluo-3. *Cytometry*. 11:923–927. https://doi.org/10.1002/cyto.990110813

Ro, T.B., R.U. Holt, A.T. Brenne, H. Hjorth-Hansen, A. Waage, O. Hjertner, A. Sundan, and M. Borset. 2004. Bone morphogenetic protein-5, -6 and -7 inhibit growth and induce apoptosis in human myeloma cells. *Oncogene*. 23:3024–3032. https://doi.org/10.1038/sj.onc.1207386

Roodman, G.D. 2004. Mechanisms of bone metastasis. *N. Engl. J. Med.* 350:1655–1664. https://doi.org/10.1056/NEJMra030831

Saneyoshi, T., S. Kume, Y. Amasaki, and K. Mikoshiba. 2002. The Wnt/calcium pathway activates NF-AT and promotes ventral cell fate in Xenopus embryos. *Nature*. 417:295–299. https://doi.org/10.1038/417295a

Sharma, S., F. Xing, Y. Liu, K. Wu, N. Said, R. Pochampally, Y. Shiozawa, H.K. Lin, K.C. Balaji, and K. Watabe. 2016. Secreted Protein Acidic and Rich in Cysteine (SPARC) Mediates Metastatic Dormancy of Prostate Cancer in Bone. *J. Biol. Chem.* 291:19351–19363. https://doi.org/10.1074/jbc.M116.737379

Shiozawa, Y., E.A. Pedersen, A.M. Havens, Y. Jung, A. Mishra, J. Joseph, J.K. Kim, L.R. Patel, C. Ying, A.M. Ziegler, et al. 2011. Human prostate cancer metastases target the hematopoietic stem cell niche to establish footholds in mouse bone marrow. *J. Clin. Invest.* 121:1298–1312. https://doi.org/10.1172/JCI43414

Siegel, R.L., K.D. Miller, and A. Jemal. 2018. Cancer statistics, 2018. *CA Cancer J. Clin.* 68:7–30. https://doi.org/10.3322/caac.21442

Sugimura, R., X.C. He, A. Venkatraman, F. Arai, A. Box, C. Semerad, J.S. Haug, L. Peng, X.B. Zhong, T. Suda, and L. Li. 2012. Noncanonical Wnt signaling maintains hematopoietic stem cells in the niche. *Cell*. 150:351–365. https://doi.org/10.1016/j.cell.2012.05.041

Syed Khaja, A.S., L. Helczynski, A. Edsjö, R. Ehrnström, A. Lindgren, D. Ulmert, T. Andersson, and A. Bjartell. 2011. Elevated level of Wnt5a protein in localized prostate cancer tissue is associated with better outcome. *PLoS One*. 6:e26539. https://doi.org/10.1371/journal.pone.0026539

Takahashi, S., T. Watanabe, M. Okada, K. Inoue, T. Ueda, I. Takada, T. Watabe, Y. Yamamoto, T. Fukuda, T. Nakamura, et al. 2011. Noncanonical Wnt signaling mediates androgen-dependent tumor growth in a mouse model of prostate cancer. *Proc. Natl. Acad. Sci. USA*. 108:4938–4943. https://doi.org/10.1073/pnas.1014850108

Takiguchi, G., M. Nishita, K. Kurita, Y. Kakeji, and Y. Minami. 2016. Wnt5a-Ror2 signaling in mesenchymal stem cells promotes proliferation of gastric cancer cells by activating CXCL16-CXCR6 axis. *Cancer Sci.* 107:290–297. https://doi.org/10.1111/cas.12871

Tetsu, O., and F. McCormick. 1999. Beta-catenin regulates expression of cyclin D1 in colon carcinoma cells. *Nature*. 398:422–426. https://doi.org/10.1038/18884

Thiele, S., A. Göbel, T.D. Rachner, S. Fuessel, M. Froehner, M.H. Muders, G.B. Baretton, R. Bernhardt, F. Jakob, C.C. Glüer, et al. 2015. WNT5A has anti-prostate cancer effects in vitro and reduces tumor growth in the skeleton in vivo. *J. Bone Miner. Res.* 30:471–480. https://doi.org/10.1002/jbmr.2362

Topol, L., X. Jiang, H. Choi, L. Garrett-Beal, P.J. Carolan, and Y. Yang. 2003. Wnt-5a inhibits the canonical Wnt pathway by promoting GSK-3-independent beta-catenin degradation. *J. Cell Biol.* 162:899–908. https://doi.org/10.1083/jcb.200303158

Torres, M.A., J.A. Yang-Snyder, S.M. Purcell, A.A. DeMarais, L.L. McGrew, and R.T. Moon. 1996. Activities of the Wnt-1 class of secreted signaling factors are antagonized by the Wnt-5A class and by a dominant negative cadherin in early Xenopus development. *J. Cell Biol.* 133:1123–1137. https://doi.org/10.1083/jcb.133.5.1123

Trowbridge, J.J., B. Guezguez, R.T. Moon, and M. Bhatia. 2010. Wnt3a activates dormant c-Kit(-) bone marrow-derived cells with short-term multilineage hematopoietic reconstitution capacity. *Stem Cells*. 28:1379–1389. https://doi.org/10.1002/stem.457

Wang, N., F.E. Docherty, H.K. Brown, K.J. Reeves, A.C. Fowles, P.D. Ottewell, T.N. Dear, I. Holen, P.I. Croucher, and C.L. Eaton. 2014. Prostate cancer cells preferentially home to osteoblast-rich areas in the early stages of bone metastasis: evidence from in vivo models. *J. Bone Miner. Res.* 29:2688–2696. https://doi.org/10.1002/jbmr.2300

Wang, N., F. Docherty, H.K. Brown, K. Reeves, A. Fowles, M. Lawson, P.D. Ottewell, I. Holen, P.I. Croucher, and C.L. Eaton. 2015. Mitotic quiescence, but not unique "stemness," marks the phenotype of bone metastasis-initiating cells in prostate cancer. *FASEB J.* 29:3141–3150. https://doi.org/10.1096/fj.14-266379

Weeraratna, A.T., Y. Jiang, G. Hostetter, K. Rosenblatt, P. Duray, M. Bittner, and J.M. Trent. 2002. Wnt5a signaling directly affects cell motility and invasion of metastatic melanoma. *Cancer Cell*. 1:279–288. https://doi.org/10.1016/S1535-6108(02)00045-4

White, D.E., N.A. Kurpios, D. Zuo, J.A. Hassell, S. Blaess, U. Mueller, and W.J. Muller. 2004. Targeted disruption of beta1-integrin in a transgenic mouse model of human breast cancer reveals an essential role in mammary tumor induction. *Cancer Cell*. 6:159–170. https://doi.org/10.1016/j.ccr.2004.06.025

Wu, T.T., R.A. Sikes, Q. Cui, G.N. Thalmann, C. Kao, C.F. Murphy, H. Yang, H.E. Zhau, G. Balian, and L.W. Chung. 1998. Establishing human prostate cancer cell xenografts in bone: induction of osteoblastic reaction by prostate-specific antigen-producing tumors in athymic and SCID/bg mice using LNCaP and lineage-derived metastatic sublines. *Int. J. Cancer*. 77:887–894. https://doi.org/10.1002/(SICI)1097-0215(19980911)77:6%3C887::AID-IJC15%3E3.0.CO;2-Z

Yamaguchi, T.P., A. Bradley, A.P. McMahon, and S. Jones. 1999. A Wnt5a pathway underlies outgrowth of multiple structures in the vertebrate embryo. *Development*. 126:1211–1223.

Yamamoto, H., N. Oue, A. Sato, Y. Hasegawa, H. Yamamoto, A. Matsubara, W. Yasui, and A. Kikuchi. 2010. Wnt5a signaling is involved in the aggressiveness of prostate cancer and expression of metalloproteinase. *Oncogene*. 29:2036–2046. https://doi.org/10.1038/onc.2009.496

Yang, Y., K. Mamouni, X. Li, Y. Chen, S. Kavuri, Y. Du, H. Fu, O. Kucuk, and D. Wu. 2018. Repositioning Dopamine D2 Receptor Agonist Bromocriptine to Enhance Docetaxel Chemotherapy and Treat Bone Metastatic Prostate Cancer. *Mol. Cancer Ther.* 17:1859–1870. https://doi.org/10.1158/1535-7163.MCT-17-1176